The Meteoritical Society

Meteoritics & Planetary Science 43, Nr 1/2, 367–397 (2008)
Abstract available online at http://meteoritics.org

Combined micro-Raman, micro-infrared, and field emission scanning electron microscope analyses of comet 81P/Wild 2 particles collected by Stardust

A. ROTUNDI[1*], G. A. BARATTA[2], J. BORG[3], J. R. BRUCATO[4], H. BUSEMANN[5, 6], L. COLANGELI[7], L. D'HENDECOURT[3], Z. DJOUADI[3], G. FERRINI[8], I. A. FRANCHI[6], M. FRIES[9], F. GROSSEMY[3], L. P. KELLER[10], V. MENNELLA[7], K. NAKAMURA[11], L. R. NITTLER[5], M. E. PALUMBO[2], S. A. SANDFORD[12], A. STEELE[9], and B. WOPENKA[13]

[1]Dip. Scienze Applicate, Università degli Studi di Napoli "Parthenope", Napoli 80133, Italy
[2]INAF-Osservatorio Astrofisico di Catania, Via Santa Sofia 78, 95123 Catania, Italy
[3]Institut d'Astrophysique Spatiale (IAS), CNRS, Université Paris-Sud, UMR8617, F-91405 Orsay-Cedex, France
[4]INAF-Osservatorio Astronomico di Arcetri, L.go E. Fermi 5, 50125 Firenze, Italy
[5]Department of Terrestrial Magnetism, Carnegie Institution of Washington, Washington, D.C. 20015–1305, USA
[6]PSSRI, Open University, Milton Keynes MK7 6AA, UK
[7]INAF-Osservatorio Astronomico di Capodimonte, Via Moiariello 16, 80131 Napoli, Italy
[8]Novaetech s.r.l., Città della Scienza, via Coroglio 57d, 80124 Napoli, Italy
[9]Geophysical Laboratory, Carnegie Institution of Washington, Washington, D.C. 20015–1305, USA
[10]NASA Johnson Space Center, Houston, Texas 77058, USA
[11]ESCG/Jacobs Engineering, NASA Johnson Space Center, Houston Texas 77058, USA
[12]Astrophysics Branch, NASA Ames Research Center, Moffett Field, California 94035, USA
[13]Department of Earth and Planetary Sciences and McDonnell Center for the Space Sciences, Washington University, Saint Louis, Missouri 63130–4899, USA
[*]Corresponding author. E-mail: rotundi@uniparthenope.it

(Submitted 12 April 2007; revision accepted 13 September 2007)

Abstract–We report combined micro-infrared, micro-Raman, and field emission scanning electron microscope (FESEM) analyses of particles collected by the Stardust spacecraft during its flyby of comet 81P/Wild 2 on 2 January 2004 and successfully returned back to Earth on 15 January 2006. We present mid-infrared (IR) spectra of six of these particles. The CH_2/CH_3 ratios inferred from the infrared data are greater than those seen in organics in the diffuse interstellar medium, possibly indicating the presence of longer or less branched aliphatic chains. The micro-Raman data offer insights into the state of the order of the carbonaceous component present in the particles. Raman parameters for most of the particles span a similar range to that observed in interplanetary dust particles (IDPs) and the most primitive meteorites. Both the IR and Raman data imply the presence of a very labile carbonaceous component. Hydrated silicates may be present in two particles of Track 35, one of which may also contain carbonates, but further investigations with other techniques need to be performed to confirm these findings. In some cases, the analyses are difficult to interpret because of the presence of compressed aerogel mixed with the grains.

INTRODUCTION

Comets are considered to be the most primitive bodies in the solar system, and for this reason they have been the targets of a number of recent space missions. After the Giotto and Vega encounters with the old (many passages close to the Sun) comet Halley in 1986 (Grewing et al. 1987) and the Deep Space 1 flyby of very old comet Borrelly in 2001 (Nelson et al. 2004), Stardust captured particles around the young comet 81P/Wild 2 on 2 January 2004 and returned them to Earth on January 15, 2006 (Brownlee et al. 2006). The returned cometary samples were collected in aerogel. On a limited number of these grains, extracted from tracks formed by the impact of the grains into the aerogel (Fig. 1), a preliminary examination was performed using a variety of analytical techniques in dedicated laboratories (see the special 2006 issue of *Science* [issue 314, #5806] and are now available for study by the general scientific community. The data presented here represent a portion of the preliminary examination (PE) effort.

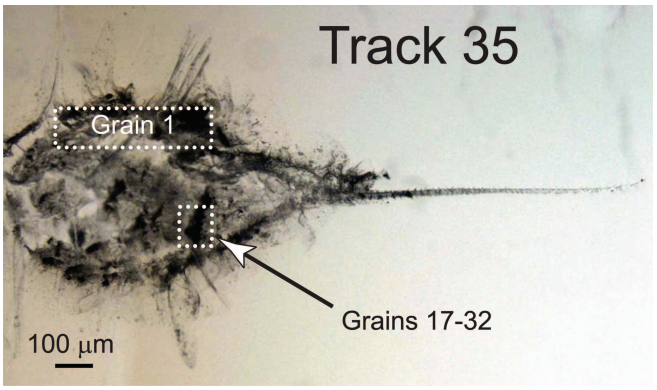

Fig. 1. An optical micrograph of Track 35. The dashed box indicates where grains from 17 to 32 were located prior to removal. Grain 1 was also located in the main "bulb" region but on the upper portion.

One of the driving forces for comet exploration is to confirm the historical theory, hypothesized by Halley, published by Newton in his *Principia* in 1686, and developed more or less continuously ever since (Anders 1989; Oró et al. 2006) that comets may have played an important role in the development of life on Earth. The extent to which comets enriched the primordial Earth with reactive C-bearing molecules and water is not known. The estimate of the endogenous contribution to Earth's organic inventory during this period is in the order of 10^8–10^{10} kg yr^{-1} (Chyba and Sagan 1997), while the flux of organic matter delivered to the Earth via comets and asteroids, averaged over the heavy bombardment period, may have been even larger at around 10^{11} kg yr^{-1} (Oró et al. 2006).

Organic molecules have been detected in some comets by previous comet flybys, e.g., comet Halley (Kissel and Krueger 1987; Fomenkova 1999), and by astronomical observations of comets like Hale-Bopp and Hyakutake (e.g., Irvine et al. 2000; Bockelée-Morvan et al. 2004; Crovisier 2004; Rodgers and Charnley 2004). The presence of C-bearing molecules in comets is to be expected based on numerous astronomical observations in which complex organic molecules have been detected, in dense molecular clouds and the diffuse interstellar medium (e.g., Sandford et al. 1991; Pendleton et al. 1994; Kuan et al. 2003; Hollis et al. 2004). Dense clouds are known to contain mixed molecular ices. The radiation processing of these ices could produce a host of organic species, including some of astrobiological interest (e.g., Bernstein et al. 1999, 2002; Dworkin et al. 2001). Molecular clouds are the parent reservoirs of protoplanetary disks, like the solar nebula, where grains were further irradiated and the effects of which may be at least as important as those occurring in the diffuse interstellar medium (ISM). This is particularly true if accretion occurred during an active phase of the young Sun (T-Tauri phase; Strazzulla et al. 1991, 2003; Gil-Hutton 2002). Organic molecules in comets could show a higher complexity than the diffuse ISM due to the reaction with fine grains of variable compositions such as ices and silicates as well as carbon grains and various molecules. Silicates act as catalysts for the reaction of organic molecules to higher complexity (Brucato et al. 2006a, 2006b). The catalytic effects of cosmic dust analogues in prebiotic reactions have been studied in the laboratory at high temperatures (Hill and Nuth 2003) and in conditions simulating the environments assumed for the early Earth (Saladino et al. 2004). A large suite of complex organic molecules have been synthesized in the gas phase on the surface of cosmic silicate dust analogues (Hill and Nuth 2003; Saladino et al. 2005).

Due to the various reaction pathways outlined above, organic molecules in minor bodies of the solar system could potentially be more complex than in the ISM. A hint to this may be seen in the difference between the CH_2/CH_3 ratio derived for the IDPs (3.7; Matrajt et al. 2005) and the considerably smaller ratio measured for lines of sight through the diffuse ISM (2.2; Sandford et al. 1991; Pendleton et al. 1994), suggesting longer aliphatic chains are present in IDPs than in the diffuse ISM. Additional differences are seen in the oxygen contents of these two types of organics. Carbon X-ray absorption near-edge structure (C-XANES) and infrared (IR) spectroscopic analyses detected significant concentrations of O in IDPs (Flynn et al. 2003; Keller et al. 2004) and in comet 81P/Wild 2 (Sandford et al. 2006; Cody et al. 2008), but IR spectral evidence indicates the organics in the diffuse ISM contain relatively little oxygen (Pendleton and Allamandola 2002; Dartois et al. 2005).

Raman spectra of disordered carbonaceous materials are dominated by two bands centered near 1360 and 1590 Δcm^{-1} (Fig. 2). The lower wave number D band (for disorder) is due to a breathing mode involving aromatic rings while the higher G band (for graphitic) is due to in-plane stretching of pairs of sp^2-bonded C atoms in both rings and chains (e.g., Ferrari and Robertson 2000). The precise position and shape of each band depends on the degree of order of the material being analyzed. With increasing ordering of the carbonaceous material, i.e., the more similar the material becomes to "disordered graphite," the widths Γ of the D and G bands decrease. So Raman spectroscopy is a complementary tool used to better understand the nature of the organics present in extraterrestrial matter.

Several studies have shown that many IDPs exhibit Raman spectra characteristic of the presence of amorphous aromatic carbon (Wopenka 1988; Raynal et al. 2001; Quirico et al. 2005; Rotundi et al. 2007). In almost all Raman analyses on IDPs, the only features seen are the amorphous carbon "G" and "D" bands superimposed upon a fluorescence background of variable intensity, although features due to minerals have been detected in a few cases (e.g., Stadermann et al. 2006; Rotundi et al. 2007). The rarity of detections of minerals in Raman spectra could be due to some combination of: a) fluorescence that masks weak features, b)

the opaque nature of the samples that prevents deep visible laser penetration, and c) the very high Raman scattering efficiency of the amorphous carbon bands G and D with respect to minerals (Quirico et al. 2005).

In this paper, we present Raman spectroscopic results obtained on 16 grains extracted from three tracks of the Stardust aerogel cometary collector. Seven of these grains were further analyzed by IR spectroscopy and/or by field emission scanning electron microscopy (FESEM), and energy dispersive X-ray analyzer (EDX). FESEM-EDX examinations provide additional information on morphology, mineralogy, and identification of C-rich entities. Our results will be compared to other primitive solar system samples like IDPs and some meteorite grains. We characterize these various samples in terms of the nature of the organic matter present, and compare our findings with what is known about organic molecules in the ISM. Preliminary reports of some of these data can be found in Sandford et al. (2006) and Keller et al. (2006).

EXPERIMENTAL

The analyses reported in this paper were performed as part of the PE phase of the returned Stardust samples (Brownlee et al. 2006). These analyses were made in a number of different laboratories on samples prepared in various ways. Details of the types of samples examined are given below and summarized in Table 1. To compare different results obtained by different groups, in particular for the Raman analyses, some preliminary cross calibrations were performed.

Sample Description and Preparation

Whole tracks in the aerogel collectors were extracted using techniques developed at the Space Sciences Laboratory, University of California in Berkeley by A. Westphal and his team (Westphal et al. 2004). Individual particles were "plucked" from these impact tracks. After extraction, the Stardust grains to be delivered to the LANDS team were deposited as bulk particles on special sample holders (SSH) (Rotundi et al. 2007). These SSHs kept the samples safe during shipment and allowed, without sample manipulation, combined micro-IR (transmission), micro-Raman, FESEM, and EDX analyses (Rotundi et al. 2007). In the SSH configuration the particles lie on a KBr window, coated with a thin Cr layer to prevent sample charging under the FESEM beam. This also secures the particles without the need for any sticking material or pressing into the KBr, thereby avoiding sample contamination and morphology modification. Other Stardust grains were pressed in gold that allows the same set of analyses, the differences being that IR data are then acquired in the reflection mode rather than in transmission mode and the original grain morphologies are modified. Two samples were microtomed thin sections, one mounted on an amorphous silicon dioxide/monoxide membrane and one mounted on gold, following sulfur embedding. The "'potted butt," remaining after the microtoming of one of these particles (17,1), was pressed in gold resulting in two small fragments (Table 1). Note that 11 of the 16 analyzed particles came from a single impact track, C2054 Track 35 (Fig. 1, Table 1).

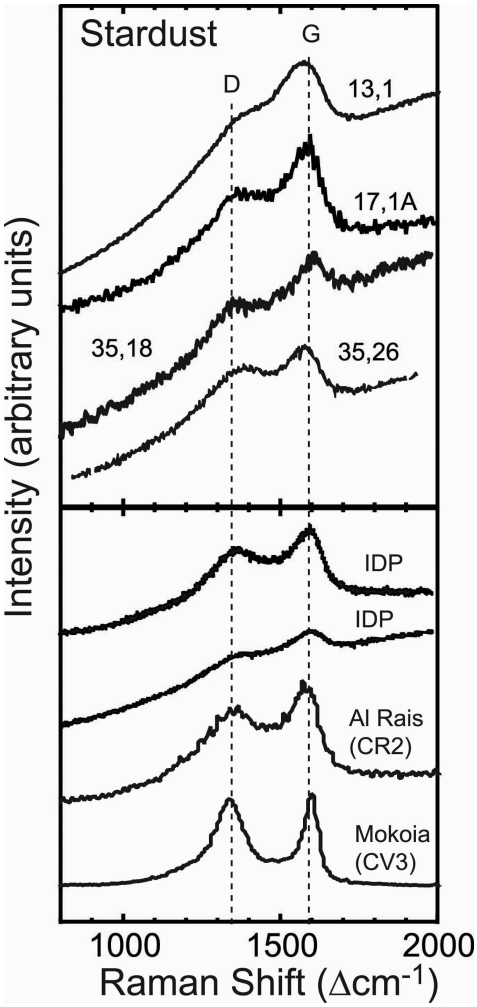

Fig. 2. Raman spectra of selected Stardust samples compared to those of interplanetary dust particles (Rotundi et al. 2007) and insoluble organic matter from two meteorites (Busemann et al. 2007). All spectra exhibit characteristic D and G bands due to disordered carbonaceous materials and fluorescence backgrounds of various intensities.

Analytical Techniques

Data were obtained using three different analytical techniques—micro-Raman spectroscopy, micro-infrared spectroscopy, and field emission scanning electron microscopy. Details of the application of these techniques to

Table 1. Stardust particles listed by aerogel cell, by track in the cell, by number of grain within the track, by analytical technique applied, by sample format, and by the team performing the analyses.

Particle # (Stardust)	Particle # (this work)	Track	Grain	Team[1]	Sample preparation	Technique
C2054,0,35,17,0	35,17	35	17	LANDS	Bulk grain deposited on KBr window	Micro-IR (transmission), Micro-Raman, FESEM/EDS
C2054,0,35,18,0	35,18		18			
C2054,0,35,20,0	35,20		20			Micro-Raman
C2054,0,35,21,0	35,21		21	IAS		Micro-IR (reflection), Micro-Raman, FESEM/EDS
C2054,0,35,26,0	35,26		26			
C2054,0,35,25,0	35,25		25	CIW	Pressed in gold	
C2054,0,35,27,0	35,27		27			
C2054,0,35,28,0	35,28		28	OU		Micro-Raman
C2054,0,35,1,0	35,1		1			
C2054,0,35,30,0	35,30		30	WU		
C2054,0,35,32,0	35,32		32	CIW	S-embedded 80 nm section on silicon dioxide/monox.	
C2044,2,41,7,0	41,7	41	7	LANDS	Bulk grain deposited onto KBr window	Micro-IR (transmission), Micro-Raman, FESEM/EDS
C2044,2,41,10,0	41,10		10			
C2044,2,41,11,0	41,11		11	CIW	Pressed in gold	Micro-Raman
FC9,0,13,1,0	13,1	13	1	CIW	Pressed in gold	
FC13,0,17,1,0	17,1A[2] 17,1B[2]	17	1A 1B			Micro-Raman, FESEM/EDS

[1]CIW = Carnegie Institution of Washington, IAS = Institut d'Astrophysique Spatiale-Orsay, LANDS = Università di Napoli Parthenope, INAF-Catania, INAF-Napoli, IOU = Open University, WU = Washington University in St. Louis.

[2]These are two fragments of the same particle.

the Stardust samples are described in the following paragraphs.

Micro-Raman Spectroscopy

All groups performed Raman analyses on their respective samples. In order to allow the inter-comparison of Stardust Raman spectroscopic results obtained in the different laboratories and assess the fitting routines used by the different groups, we performed two systematic tests: (1) all groups reduced a set of simulated Raman spectra using procedures as close as possible to the protocols outlined hereafter used for the Stardust samples; (2) all groups analyzed small fragments of meteoritic Insoluble Organic Matter (IOM) extracted from three meteorites, the primitive carbonaceous chondrite (CC) Cold Bokkeveld (CM2), the intermediate CC Leoville (CV3.0), and the thermally metamorphosed CC Allende (CV3.2) (Alexander et al. 2007). The three meteorite IOM samples were relatively homogeneous, and their average D and G band parameters are distinctly different, as one would expect due to the different degrees of metamorphism those meteorites experienced (Busemann et al. 2007). Hence, they are well suited for inter-laboratory comparisons. The details of these calibrations can be found in Appendix A.

Raman spectra were taken by the LANDS (Laboratory Analyses of Dust from Space) team at the Laboratorio di Astrofisica Sperimentale, Catania using a continuous multi-line Ar ion laser beam at 514.5 nm wavelength. A confocal microscope (DILOR) focuses the laser beam onto the particle in a 1 μm diameter spot with a power mostly maintained at 0.03 mW and always lower than 0.1 mW. The Raman scattered light arising from the illuminated spot is collected by the same objective and is collimated into a parallel beam that is reflected back along the same path of the laser. The Raman scattered light is then focused on the entrance slit of the triplemate spectrometer (SPEX) equipped with a CCD detector, allowing measurements with negligible performance losses (Rotundi et al. 2007). The spectral resolution used for Stardust particle was 8 Δcm^{-1} with a peak accuracy of 1 Δcm^{-1}. The D and G features were fitted with two Lorentzian bands and a linear baseline.

Raman spectra were obtained by the Orsay-Institut d'Astrophysique Spatiale (IAS) team with a Labram HR800 Horiba Jobin-Yvon spectrometer (national facility equipment at Ecole Normale Supérieure, Lyon). Excitation is delivered by an argon ion laser (514.5 nm) and the spectral resolution is 1 Δcm^{-1} when using a 1800 gr/mm grating. The laser power at the sample surface did not exceed 0.1 mW. The spatial resolution is 1 mm using a ×100 Olympus objective. The analytical procedure consisted of fitting the D and G bands with two Lorentzian bands and a linear baseline.

Raman analyses made at the CIW were performed with a multi-function scanning probe microscope. The instrument, a

WiTec α-SNOM, includes near-field optical microscopy and confocal imaging Raman microscopy (532 nm frequency-doubled Nd:YAG laser). The instrument allows Raman characterization of samples with sub-μm spatial resolution (typically ~400 nm with ×100 short working distance objective), at low power (0.055 mW measured at the focal plane). Spectral images were acquired, where each pixel contains a full Raman spectrum (1024 channels, 600 gr/mm, ~4 Δcm^{-1} spectral resolution, typically 3–4 s/pixel). Fluorescence is reduced with the use of confocal optics. The Raman data cube was reduced using custom software, and the D and G bands were fitted with two Lorentzian profiles and a linear background.

Raman images are produced by first obtaining a full spectrum (from 100–3500 Δcm^{-1}) from each individual $(360\ nm)^2$ spot. In order to do this, the sample is being continuously moved ("rastered") under a stationary excitation beam and thousands of full spectra of adjacent $(360\ nm)^2$ spots are acquired. With a dwell time of 6 s per spot, the complete spectral acquisition of a total area of 10 × 10 μm thus takes about 1.3 h. After the spectral acquisition is accomplished, the relative intensities of individual selected peaks can be imaged and graphically displayed with the appropriate software.

Laser Raman analyses at PSSRI, Open University (OU) were conducted with a Horiba Jobin Yvon Labram HR Raman system. Excitation is delivered by an argon ion laser (514.5 nm) and the spectral resolution is 3 Δcm^{-1} when using a 600 gr/mm grating. The laser delivered a power at the sample surface of 0.18 mW (grain 35,28) and 0.06 mW (grain 35,1). The beam was focused with a ×100 long working distance objective giving a spatial resolution of approximately 1 μm. Spectra were recorded across the whole of each particle with a 1.5 μm step in both x and y. Spectra were accumulated as 5 sets of 30-second integrations. The steep sloping fluorescence baseline was subtracted and the D and G features fitted with a Gaussian-Lorentzian model.

Raman measurements at Washington University (WU) in St. Louis were performed with an integrated, fiber-optically coupled microscope-spectrometer-detector system (HoloLab Series 5000 Raman Microscope from Kaiser Optical Systems, Inc). This instrument has no moving parts and is based on an axial spectrometer with holographic gratings that allows for very good photon efficiency and wavelength accuracy. Raman excitation light of 532 nm is delivered by a frequency-doubled Nd-YAG laser that was coupled into a Leica microscope via a 8 μm single mode optical fiber. A 80× ULWD objective with NA of 0.75 and a working distance of 8 mm was used for focusing the light onto the sample, which resulted in a spatial resolution of ~1 μm. The laser power at the surface of the sample was less than 0.5 mW. The spectral range of 100–4000 Δcm^{-1} was simultaneously detected with a thermoelectrically cooled CCD array detector with 2048 channels and a spectral resolution of 2.5 Δcm^{-1}. Spectral acquisition time was 64 × 4 s per spectrum. Data acquisition, intensity and wavelength calibration, as well as filtering were controlled by the HoloGrams software. Peaks were deconvolved with a Lorentzian algorithm and a linear baseline correction.

Micro-Infrared Spectroscopy

Infrared spectra were obtained by two laboratories (LANDS-Napoli and IAS-Orsay) on the same samples as studied by Raman spectroscopy. Infrared spectra were acquired by the LANDS team at the Laboratorio di Fisica Cosmica e Planetologia (LFCP), Napoli, with a microscope attached to a FTIR interferometer (Mod. Bruker Equinox-55) in the range 7000–600 cm^{-1} and a spectral resolution of 4 cm^{-1}. Comet Wild 2 particles were analyzed on KBr windows in transmission mode. The smallest infrared beam focused on the samples was around 20 μm, slightly larger then the maximum elongation of the analyzed particles. The IR source is an internal globar type source; KBr beam splitters are available in the 5000–500 cm^{-1} range.

The Orsay-IAS group used a NicPlan microscope in the reflection mode, associated with the Magma 860 FT-IR spectrometer equipped with MCT detectors, for analyzing particles pressed in gold. The IR source is an internal globar type source; KBr beam splitters are available in the 5000–500 cm^{-1} range. The wavelength/wave number coverage is 4000–650 cm^{-1} (2.5–15.4 μm) with a spectral resolution of 4 cm^{-1}. The smallest infrared beam focused on the samples was around 15 μm large, the approximate size of the samples.

Field Emission Scanning Electron Microscopy

Both LANDS and IAS completed their spectroscopic investigation with an analysis of the same grains by FESEM techniques. Morphologies of Stardust grains were determined by the LANDS team at the LFCP, Napoli, using a ZEISS Supra FESEM. Low accelerating voltages from 3 kV to 5 kV were used to maximize the resolution with respect to the charging of the uncoated particles to avoid sample contamination. The EDX analysis was performed using an Oxford INCA Energy 350 system attached to the FESEM with a Si(Li) INCA X-sight "PREMIUM" detector at an accelerating voltage of 15 kV. In spot mode the analyzed region can be approximated by a cube of about 1 μm on a side.

The electron microscopy studies of the IAS team were performed at the Laboratoire de Structure et Propriétés de l'Etat Solide (LSPES) in Lille, France. FESEM was accomplished on a SZM-FEG Hitachi S4700 microscope and images were obtained in secondary electron (SE) mode at an acceleration voltage of 30 kV. The SE detector is located inside the lens allowing high resolution images. Chemical analyses were performed with the EDX available on the

microscope (Noran-Voyager) recorded as spectra of select regions of interest. For quantification, the PROZA procedure was used (close to a ZAF procedure) for flat samples.

A JEOL 6500F FESEM was used at CIW for characterization of Stardust samples prior to Raman analysis. EDX measurements were made with an EDAX Genesis system.

RESULTS AND DISCUSSION

Micro-Raman Spectroscopy

The only features clearly identified in all our micro-Raman spectra of samples from comet 81P/Wild 2 particles are the aromatic D and G bands (around 1360 and 1590 Δcm^{-1}) superimposed onto a fluorescence background of variable intensity (Fig. 2). These first-order D and G bands are characteristic of carbonaceous materials with a wide range of crystalline order (Tuinstra and Koenig 1970) and are commonly observed in both terrestrial and extraterrestrial samples (Wopenka 1988; Pasteris and Wopenka 1991; Beyssac et al. 2003; Quirico et al. 2003; Raynal 2003; Pasteris and Wopenka 2004; Quirico et al. 2005; Schopf et al. 2005; Bonal et al. 2006; Rotundi et al. 2007; Busemann et al. 2007; Court et al. 2007). The precise position and shape of each band depends on the degree of order of the material being analyzed. The widths Γ of the D and G bands decrease with increasing ordering (i.e., annihilation of defects, removal of heteroatoms and decreasing distortions of the threefold coordinated C atoms from the ideal structure of graphite) of the carbonaceous material. The D band position ω_D follows a nonlinear trend with crystalline order as noted elsewhere (Busemann et al. 2007). With increasing order ω_G increases from regions with low ω_G, typical for highly amorphous C (see Amorphization section), towards ω_G values around 1600 Δcm^{-1} (Ferrari and Robertson 2000). The development of a weak second D band (D') at ~1620 Δcm^{-1}, which is usually unresolved from the G band, alters the apparent ω_G to a small degree. For graphite, defined as an ordered crystalline domain of pure carbon that is large with respect to the laser excitation wavelength, ω_G is exactly at 1582 Δcm^{-1}.

Cross Calibration of Results from Different Laboratories

Generated Spectra

The various routines used by the five groups give consistent results (Table A1) for the simulated Raman spectra (see Appendix A), indicating that none of the fitting procedures to obtain the Raman D and G band parameters used in the distinct laboratories add additional errors that would preclude inter-laboratory comparison of the results from the analyses of the extraterrestrial organic samples. However, steep backgrounds underlying the D and G bands can cause significant divergence of the fitted parameters from the true values, particularly Γ_D and Γ_G. Those spectra most difficult to fit yield Γ_D and Γ_G parameters that deviate by up to 110 cm^{-1} from the input parameters. However, the spread of Γ_D and Γ_G, determined by the different laboratories, is in all but one cases <16 cm^{-1}. Random noise added to small peaks or steep backgrounds results in small shifts of the peak positions. The peak positions ω determined in the various laboratories agree with each other in almost all cases within 0.8 cm^{-1}, whereas the systematic deviation from the input parameter is usually <2 cm^{-1} and reaches 12 cm^{-1} in one case. The broader D bands are more affected by this problem than the G bands.

Meteoritic Insoluble Organic Matter (IOM)

The Raman parameters for meteoritic IOM of Cold Bokkeveld, Leoville, and Allende are correlated with the different degrees of thermal metamorphism experienced on the meteorite parent bodies (Raynal 2003; Quirico et al. 2003; Matrajt et al. 2004; Quirico et al. 2005; Bonal et al. 2006; Busemann et al. 2007). Table A2 gives the results in all laboratories of the Raman parameters as measured for meteoritic IOM including the standard deviations. The analyses in all five laboratories yielded comparable results for Γ_D, Γ_G, and ω_G. A downshift of 3–4 Δcm^{-1} in primitive IOM is observed for ω_D measured at CIW with 532 nm laser light compared to the results from most other laboratories. Even though the discrepancy is small (~5 and 2 cm^{-1} for Cold Bokkeveld and Leoville, respectively), and can in part be explained due to the different laser excitation wavelengths, it does suggest results from different laboratories should be compared with caution.

Overall, however, uncertainties due to inter-laboratory comparison are small compared to the observed natural variations in Stardust organic matter (see next section). As a rough measure, Table A2 gives the standard deviations of the Raman parameters as measured for meteoritic IOM taking into account the results of all five laboratories using two different laser excitation wavelengths. We see some differences between the groups, but they are not large enough to change any of the main conclusions described in the following discussions.

D and G Bands of Stardust Particles: The Degree of Carbon Order in Stardust Particles Compared to IDPs and Meteorites

As stated previously, Raman spectra of Stardust particles are dominated by the D and G bands centered around 1360 and 1590 Δcm^{-1} (Fig. 2). A few particles show spectra that differ somewhat, however. In three cases (particles: 35,32; 41,11 and 35,30) the spectra contain additional aliphatic C–H features (see Aliphatic section) and another three (particles: 41,10; 41,7 and 35,25) they exhibit G and D bands that can barely be distinguished above the background noise (Table 2). The lack of detection of minerals and specific organics features other than the D and G bands could be due to masking effects of fluorescence and/or to the opaque nature of the samples preventing deep laser penetration (>100 nm)

Table 2. D and G band parameters (ω = center; Γ = full width at half maximum) derived from Raman spectra of Stardust samples. Errors in most cases represent the standard deviation of results from multiple measurements of a given sample. Note that grains 41,7; 41,10; 41,11; and 35,25 (Table 1) exhibited the D and G bands but spectra were of insufficient quality to quantitatively extract parameters.

Particle # (track, grain)	Team	ω_D (±1σ)	Γ_D (±1σ)	ω_G (±1σ)	Γ_G (±1σ)
35,20	LANDS	1366.1 ± 5.7	278.1 ± 27	1599.0 ± 2.7	105.9 ± 10
35,18		1351.1 ± 3.3	245.55 ± 15	1594.54 ± 2	122.4 ± 8
35,17		1361.6 ± 2.1	378 ± 31.2	1576.1 ± 1.2	125.1 ± 3.5
35,21	IAS	1374 ± 3	316.5 ± 20.9	1582.1 ± 5.2	96 ± 9.7
35,26		1371.8 ± 2.6	318.4 ± 25.2	1585.2 ± 1.5	135.5 ± 12.2
35,28	OU	1356.3 ± 4.3	297.3 ± 36.1	1595.2 ± 2.2	109 ± 7.8
35,1		1372.4 ± 13.5	333.8 ± 36.3	1589.3 ± 3.3	142.3 ± 32.9
35,30	WU	1351.9 ± 3.2	204.4 ± 16.8	1591.9 ± 1.4	84.4 ± 7
35,27		1346 ± 5	267 ± 20	1585 ± 3	94 ± 11
35,32		1344.5 ± 5.6	312 ± 43	1601 ± 5	72 ± 14
13,1		1372 ± 4	392 ± 12	1567 ± 1	143 ± 5
17,1A		1369 ± 2	319 ± 9	1581.5 ± 0.8	114 ± 3
17,1B		1357 ± 10	311 ± 13	1578 ± 2	120 ± 4

into the samples. In addition, the very high Raman scattering efficiency of the amorphous carbon with respect to covalent bonds in minerals and other chemical bonds in organic matter generally causes the D and G bands to dominate the spectra (Quirico et al. 2005). This is particularly true for visible laser excitation as used here due to resonance of the sp^2 carbon sites.

D and G band parameters derived from the Stardust spectra as those reported in Fig. 2 are given in Table 2 and compared in Fig. 3 to those observed in other extraterrestrial materials, such as IDPs, primitive meteorites and IOMs extracted from meteorites. Note that some of the G band parameters differ slightly from those presented graphically by Sandford et al. (2006) due to minor refinement of data analysis techniques. Although the band intensity ratio I_D/I_G is often discussed as a useful parameter, this ratio is nonlinear with respect to metamorphic history when viewed over a wide range of values, as both very thermally processed carbonaceous materials and very disordered materials can show similar I_D/I_G values (Busemann et al. 2007). Thus, we concentrate here only on the band centers (ω) and widths (Γ). For most samples, uncertainties represent the standard deviations of parameters determined for multiple spots, though in a few cases errors are dominated by counting statistics. Most samples were individual grains (Table 1); eleven extracted from along Track 35 (Fig. 1), two from Track 41, and two terminal particles from Track 13 and Track 17, the former as a microtomed slice (Fig. 4) and the latter as two fragments of a thick remnant of the microtomed grain (see Stardust Online Catalog: http://curator.jsc.nasa.gov/stardust/sample_catalog/index.cfm for full description of tracks).

The D and G band parameters depend on the degree of structural disorder and chemical impurity in carbonaceous materials. Organic matter in meteorites and IDPs follows systematic trends on plots of band position versus width, according to the degree of primitiveness inferred by other means, e.g., isotopic anomalies and mineralogical characteristics, (Busemann et al. 2007). The Stardust samples follow similar trends and span almost the entire range of parameters previously observed in meteorites and IDPs (Fig. 3).

In Fig. 3 the G and D band parameters of Wild 2 samples relative to IOM from a large number of meteorites (squares) from different classes (Busemann et al. 2007; Cross Calibration section) and some IDPs are compared. The shaded regions in Figs. 3c and 3d show the range of parameters observed in chemically unprocessed (i.e., without extraction) meteorites of different types (Raynal 2003; Quirico et al. 2003, 2005; Bonal et al. 2006).

The dashed line in Figs. 3c and 3e illustrates a rough trend obtained for the IOM G band data at CIW. Many of the chemically unprocessed meteorite data lie significantly to the right of the IOM trend. This might reflect a contribution of soluble carbonaceous materials with different Raman properties in the chemically unprocessed samples, as well as differences in experimental setup and data analysis procedures between the different studies (Busemann et al. 2007).

The general behavior of meteoritic organic matter in Raman parameter plots is consistent with the general behavior expected for disordered carbon as outlined above. For the G band, organics from the most primitive meteorites (e.g., CI, CR, and CM chondrites) show low band centers and large band widths, indicating very disordered materials. Organic matter from more thermally processed meteorites (e.g., UOCs and CVs) show higher band centers (up to and exceeding 1590 Δcm^{-1}) and narrower peaks. Meteorites containing graphite (e.g., enstatite chondrites) show even smaller band widths (≤50 cm^{-1}) and G band positions near 1582 Δcm^{-1}. Some of the most primitive IOM samples and some Stardust samples have G band centers that are unusually

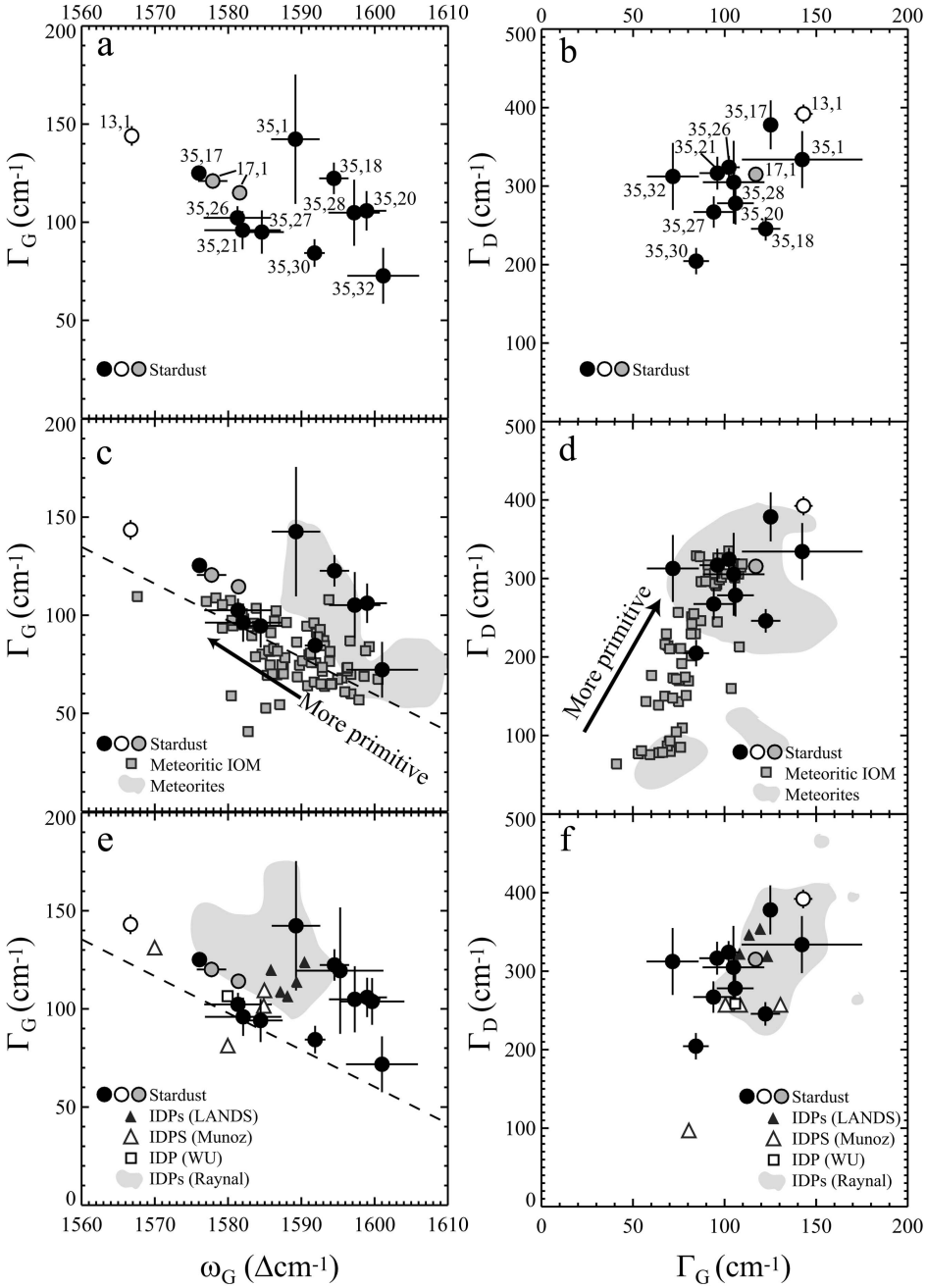

Fig. 3. Raman D and G band parameters (ω = center; Γ = full width at half maximum) of Stardust samples compared to those of meteorites and interplanetary dust particles (IDPs). a, b) Stardust data. c, d) Stardust data compared to meteorites. "IOM" is insoluble organic matter separated from wide range of meteorite classes (Busemann et al. 2007). Gray regions show the range of parameters measured in chemically unprocessed meteorites (Quirico et al. 2003; Raynal 2003; Quirico et al. 2005; Bonal et al. 2006). e, f) Stardust data compared to interplanetary dust particles (IDPs). The "LANDS" data are from Rotundi et al. (2007), the " Muñoz" data are from Muñoz-Caro et al. (2006) and the WU IDP data point is from Stadermann et al. (2006). Gray regions indicates range of IDP data reported graphically by Raynal et al. (2001). In (c) and (e) the long-dashed line is fit to the IOM data of Busemann et al. (2007). For clarity, only the average of the two (similar) Track 17 samples is shown in (d–f).

low (e.g., <1580 Δcm^{-1}) for carbon samples of any origin. While sample heating is known to produce this effect (Everall and Lumsdon 1991), careful control of laser power and calibration of heating effects conducted among participating laboratories discounts this possibility. As discussed in more detail in the next section, amorphization due to irradiation can lead to such low values for ω_G. Moreover, addition of heteroatoms like O or N can also cause down-shifting of G band centers in poorly ordered carbonaceous materials (e.g., Neuhaeuser et al. 2000). Potential evidence for this in the most disordered Stardust sample (Track 13) is discussed below.

Most primitive meteorites show very wide D bands (≥300 cm^{-1}, Fig. 3d) and relatively high band centers (see IOM in Table A2). Meteorites that have experienced more thermal processing show narrower D bands and lower D band centers compared to unprocessed meteorites.

Raman band parameter data for IDPs collected in the stratosphere (Bradley 2003; Brownlee 2003) are compared with the Stardust data in Figs. 3e and 3f. These IDP data were acquired in some of the same laboratories as were the Stardust data, though analytical conditions and data analysis procedures were not necessarily identical (Raynal et al. 2001; Muñoz-Caro et al. 2006; Rotundi et al. 2007). The grey areas indicate the range of IDP data reported graphically by Raynal et al. (2001). IDPs almost certainly originate from both comets and asteroids (Brownlee et al. 1995; Rietmeijer 2002; Keller and Messenger 2005), although a specific source type for any specific particle cannot unambiguously be identified. They are considered to be among the most primitive extraterrestrial materials available for study in the laboratory. IDPs are highly unequilibrated aggregates of nanoscale phases, have high C contents, and have high abundances of isotopically anomalous presolar grains and organic matter. Interestingly, the IDPs exhibit Raman D and G band parameters that span and extend beyond the ranges observed in meteorites of different classes, indicating a previously unsampled range of origins and/or thermal histories (Raynal et al. 2001).

Most of the Stardust data lie near the IOM G band trend, while a few (mostly with large errors) overlap with the primitive in situ meteorite data. The D and G band widths of the Stardust data lie at the primitive end of the meteoritic trends (Fig. 3d). For both D and G bands, the Stardust data cover a remarkably similar range to those of IDPs, perhaps strengthening the association of the latter with comets. In the following some of the Stardust grains are discussed in detail, ordered according to the tracks in which they were found.

Eleven of the 16 analyzed samples were picked from a single impact track (Track 35) in the Stardust aerogel collector (Fig. 1). These individual grains span a relatively wide range of D and G band parameters, comparable to that observed for primitive meteorites and IDPs, indicating a heterogeneous assortment of carbonaceous structures. All but one of the particles originated in a small region of the aerogel impact track (Fig. 1), so it is not possible to infer a correlation between Raman band parameters and the position of a given particle within the overall track. Most of the Track 35 grains that were analyzed by FESEM/EDX were found to include large amounts of melted aerogel with some traces of Mg and Fe originally present in cometary silicates, as well as varying amounts of C, S, and Ca (see Micro-IR, FESEM/EDX section). In view of the heating experienced by these grains, it is somewhat astonishing that the carbonaceous materials they contain exhibit varying band parameters comparable to primitive meteorites and IDPs. However, we want to recall here that there is evidence of melted (thus heated) aerogel, but no evidence of bulk grain heating. It is thus possible that the grain was not transformed too much by the slowing down in the aerogel and the heating that melted the aerogel did not completely transform the pre-existing carbonaceous materials. Studies of the alteration of organics upon impact of Allende, Murchison, and Orgueil samples with impact velocity of 6.1 km/s into aerogel showed that only the Orgueil D band position (ω_D) lowered after impact, whereas all other parameters did not vary (Foster et al. 2007). Even if some of the observed range was due to short term heating during impact into the aerogel, this heating was clearly heterogeneous and was less severe than the long period parent body heating experienced, e.g., by organic matter in CV chondrites (which typically have $\omega_G > \sim 1590\ \Delta cm^{-1}$ and $\Gamma_D < \sim 80\ cm^{-1}$) (this work Table A2; Bonal et al. 2006; Busemann et al. 2007). Note that grain 35,17 that shows evidence for hydrated silicates and carbonates (see Micro-IR, FESEM/EDX section), also exhibits some of the most primitive Raman signatures of any of the analyzed samples.

Grain 13,1 was extracted from a loose chip of aerogel found on the avionics deck within the sample return canister; its original position on the aerogel collector tray is therefore unknown. The particle was embedded in elemental S and sliced with a diamond microtome. SEM analysis of the 0.5 mm thick slice indicated it to be almost pure C with minor O (Fig. 4) and the sample showed a distinctly disordered C Raman spectrum (Fig. 2). The band parameters place it beyond the most extreme primitive ends of the trends defined by meteoritic IOM. In fact, the Raman spectrum resembles that of amorphous carbon like that produced by irradiation of carbonaceous materials (Ferrini et al. 2004), namely the D and G bands have almost merged into a single broad hump (see next section for more discussion). This slice was also found to be enriched in deuterium, with D/H about twice the terrestrial value (McKeegan et al. 2006), which excludes a contamination origin for this grain. Moreover, C-XANES analysis (Sandford et al. 2006; Cody et al. 2008) of adjacent slices of this particle indicated lower abundances of sp^2-bonded C and higher N/C and O/C ratios than observed in typical chondritic organic matter. For example, IOM from carbonaceous chondrites has O/C = 0.04–0.22 and N/C up to 0.04, whereas the 13,1 particle has O/C and N/C ratios of 0.21 ± 0.01 and 0.10 ± 0.03, respectively (Cody et al. 2008). As discussed above, this high level of heteroatom abundance might be partially related to the very low G band center observed for this sample. Further research into the effects of heteroatom concentration on Raman bands of extraterrestrial carbonaceous materials including more Stardust samples is necessary for definitive evaluation, however.

TEM analyses of grain 17,1, indicate a heterogeneous

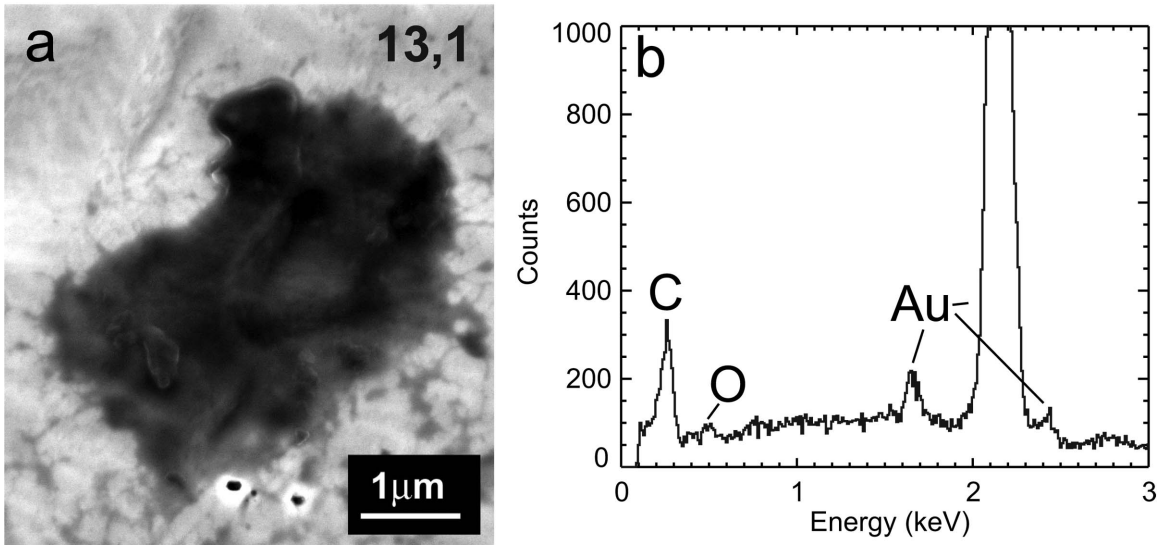

Fig. 4. a) Scanning electron micrograph of 500 nm thick microtome slice of grain 13,1 analyzed by Raman spectroscopy. b) Energy dispersive X-ray spectrum of grain 13,1, showing only peaks due to C, O and Au (from the substrate).

assortment of grains, including pyroxene, olivine, and sulfides (see Stardust sample catalog). The Raman spectra of two small fragments of the potted butt following microtoming (see Experimental section) clearly indicated the presence of C and gave roughly similar results at the primitive end of the D and G band trends (Fig. 3). This grain also was found to be D-rich, with D/H about twice terrestrial (McKeegan et al. 2006).

The Amorphous Carbon Raman Features of Stardust Particles: Comparison with Laboratory Analogs and Ion Irradiated Carbons

Once formed, comets are exposed to the flux of solar, heliospheric, and galactic cosmic rays. For instance, it has been estimated that the external layers (0.1–0.5 m) of an Oort cloud comet are subjected in the life time of the comet of 4.6×10^9 yr to an irradiation dose of 600 eV/molecule by galactic cosmic rays that could lead to the formation of a substantial crust (Strazzulla and Johnson 1991; Strazzulla et al. 1991, 2003). Estimated irradiation doses for objects in the classical Kuiper Belt at 40–50 AU are generally lower and may marginally produce an outer web of devolatilized material (Strazzulla et al. 2003); nevertheless, doses are still sufficient to produce irradiation mantles several meters thick where significant chemical changes can occur (Gil-Hutton 2002). Even for deep layers within the nucleus, irradiation effects might not be irrelevant since grains could have been irradiated significantly in the ISM before solar system formation. Furthermore, even very deep layers could have been irradiated significantly in the solar system if the active T-Tauri phase of the young Sun, occurred before the comets accreted (Strazzulla and Baratta 1992). Thus, it is interesting to study in the laboratory the effects of ion irradiation on astrophysical analogues and compare the results with observations on extraterrestrial materials.

Raman spectroscopy has often been used to study the effects of ion-induced lattice damage in carbonaceous solids and organic compounds (e.g., Elman et al. 1981; Strazzulla and Baratta 1992; Baratta et al. 1996; Musumeci et al. 2000; Strazzulla et al. 2001; Baratta et al. 2004; Palumbo et al. 2004; Ferrini et al. 2004). In particular, the effects of ion irradiation have been studied on ice made of benzene (C_6H_6), butane (C_4H_{10}), methane (CH_4), and mixtures such as H_2O:CH_4:N_2 (Strazzulla and Baratta 1992; Ferrini et al. 2004; Palumbo et al. 2004). Raman spectra of icy samples have been taken at low temperature (about 12 K) before and after ion irradiation, after warm up of the irradiated samples to room temperature, and after irradiation at room temperature. These spectra show that the initial ice is partially converted into a refractory residue, which, under further irradiation, evolves towards an amorphous carbon which is often referred to as "ion-produced hydrogenated amorphous carbon" (IPHAC). The IPHAC formation has been observed not only in carbon containing irradiated ices but also in refractory materials such as polymers, PAHs, fullerenes, etc. (Cannia et al. 1994; Cataldo et al. 2003). We would like to note that, although the IPHAC formation is a general process, the efficiency of amorphous carbon formation and its structure depend on the starting material. In particular, the effects of radiation in organic matter are various and depend on organic starting material complexity and the presence of water (Court et al. 2006).

Amorphous carbon (AC) grains have been produced by arc discharge between two amorphous carbon electrodes in an inert Ar atmosphere. Electron microscopy studies revealed that they consist of spheroids with average radii of 5 nm arranged in fluffy aggregates (Rotundi et al. 1998; Rietmeijer

et al. 2004). Infrared spectroscopy has shown that the AC grains contain hydrogen (–CH3 and –CH2, H/C ~ 4%) and a small amount of oxygen (O/C < 0.5%) (Baratta et al. 1996). Raman spectra of AC grains irradiated with 3 and 30 keV He^+ ions at different fluences (Baratta et al. 1996; Mennella et al. 2003) imply a progressive decrease in the I_D/I_G ratio and a shift of the G band peak towards lower wave numbers. These results are interpreted as evidence of a progressive disorder induced by ion irradiation in AC grains.

Raman spectra of "highly ordered pyrolitic graphite" (HOPG), irradiated with 3 keV He^+ ions at different ion fluences, show that ion irradiation at low fluences induces damage in the crystal lattice, as evidenced by the appearance of an increasing D band. At higher fluences (>10^{16} ions cm^{-2}), the damaged graphite crystal is fully converted into an amorphous carbon film (Compagnini and Baratta 1992; Strazzulla et al. 1995), showing that ions are able to amorphize even highly ordered crystalline materials as graphite.

In Fig. 5, irradiated AC (IPHAC, formed after ion irradiation of icy samples) plots in the top left corner of the graph. For graphite and AC grains increasing ion irradiation fluences shift the G band to lower wave numbers and higher Γ, while metamorphism causes a modification of the G band profile in the opposite direction (Bonal et al. 2006; Busemann et al. 2007). The plot shows that Stardust grains are compatible with the presence of amorphous carbonaceous materials that have been slightly irradiated. The most disordered AC in some Stardust grains (e.g., particle 13,1) could be indicative of ion irradiation of pre-existing, initially more ordered carbons or carbon containing ices (IPHAC) that had suffered moderate metamorphism.

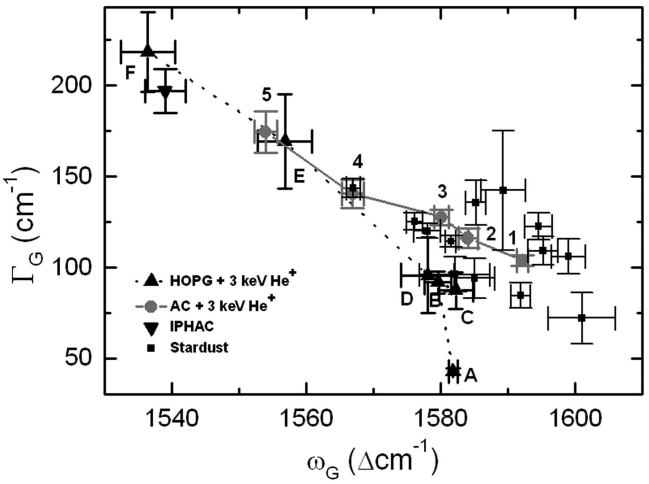

Fig. 5. Full width at half maximum (Γ_G) versus peak position (ω_G) of the G band observed in Stardust grains compared with ion processed materials. Up triangles correspond to HOPG irradiated with 3 keV He^+ ions at different fluences (ions cm^{-2}): (A) 2.8×10^{13}; (B) 1.2×10^{14}; (C) 2.8×10^{14}, (D) 1.4×10^{15}; (E) 1.4×10^{16}; (F) 2.8×10^{16}. Solid gray circles refer to amorphous carbon (AC) grains irradiated with 3 keV He^+ ions. Numeric labels indicate different irradiation fluences (ions cm^{-2}), in particular (1) virgin; (2) 10^{14}; (3) 10^{15}; (4) 10^{16}; (5) 10^{17}. The down triangle refers to amorphous carbon (IPHAC) produced by ion irradiation of an ice mixtures made of H_2O:CH_4:N_2 = 1:6:3 with 30 keV He^+ ions at 12 K (irradiation dose = 800 eV/molecule).

Aliphatic Hydrocarbons Detected with Raman Spectroscopy

In addition to the broad D and G Raman bands, three particles also revealed Raman bands in the C-H stretching region (~2900 Δcm^{-1}) indicative of aliphatic components. Such aliphatic signatures were revealed both by Raman imaging (Fig. 6a) as well as by spot analysis (Fig. 6b: spectra 1–4). Two of the particles were from Track 35 in Cell 2054 (particle 32 and particle 35) and one particle was from Track 41 in Cell 2044 (particle 11). Particle 35,32 was embedded in sulfur and microtomed, whereas particles 35,30 and 41,11 were pressed in gold (see Experimental section). Examples of spectra obtained on all three particles are shown in Fig. 6b.

In principle, one can infer the general nature and composition of aliphatics from the exact positions and shapes of the 2800–3100 Δcm^{-1} C-H stretching modes. Those positions and shapes are observed to be different for the three different Stardust particles (compare spectra 1, 2, and 4 in Fig. 6b), and also differ slightly among different (360 nm)^2 spots within the same particle. Particle 35,30 showed very strong peaks for the C-H stretching vibrations at 2848 and 2882 Δcm^{-1} and an additional unusual weak band at 1439 Δcm^{-1} (Fig. 6b, spectrum 1), consistent with the presence of alkane-type saturated hydrocarbons. Those bands cannot be caused by aromatic C-H stretches, because such modes would be at much higher wave numbers (>3000 Δcm^{-1}). The detection of these bands was possible after sample 35,30 was photo-bleached with the 532 nm laser beam for one hour, which decreased the overall fluorescence background. The bands are characteristic of an alkane, in which the C=H symmetric stretching vibration for methyl (CH_3) is found at 2888 Δcm^{-1} and the symmetric C=H stretching vibration for methylene (CH_2) is found at 2849 Δcm^{-1}. An additional small band at 1439 Δcm^{-1} is probably caused by the methylene wagging mode. However, alkanes with such a spectrum have to be either (1) very high molecular weight alkanes (if they are mixed with PAH-like condensed carbon ring structures), because lower weight alkanes (i.e., short chains) would be in the form of a gas or a liquid, or (2) alkanes in which the chains can be shorter (i.e., low molecular weight alkanes) as long as they are side chains of the PAHs and form alkylated PAHs. The fact that the observed bands are a good match to the strongest bands expected for polyethylene (Sandford et al. 2006) raises the question whether the cause of those bands could be contamination.

The other two particles (35,32 and 41,11) were measured with a different Raman instrument and did not have such well

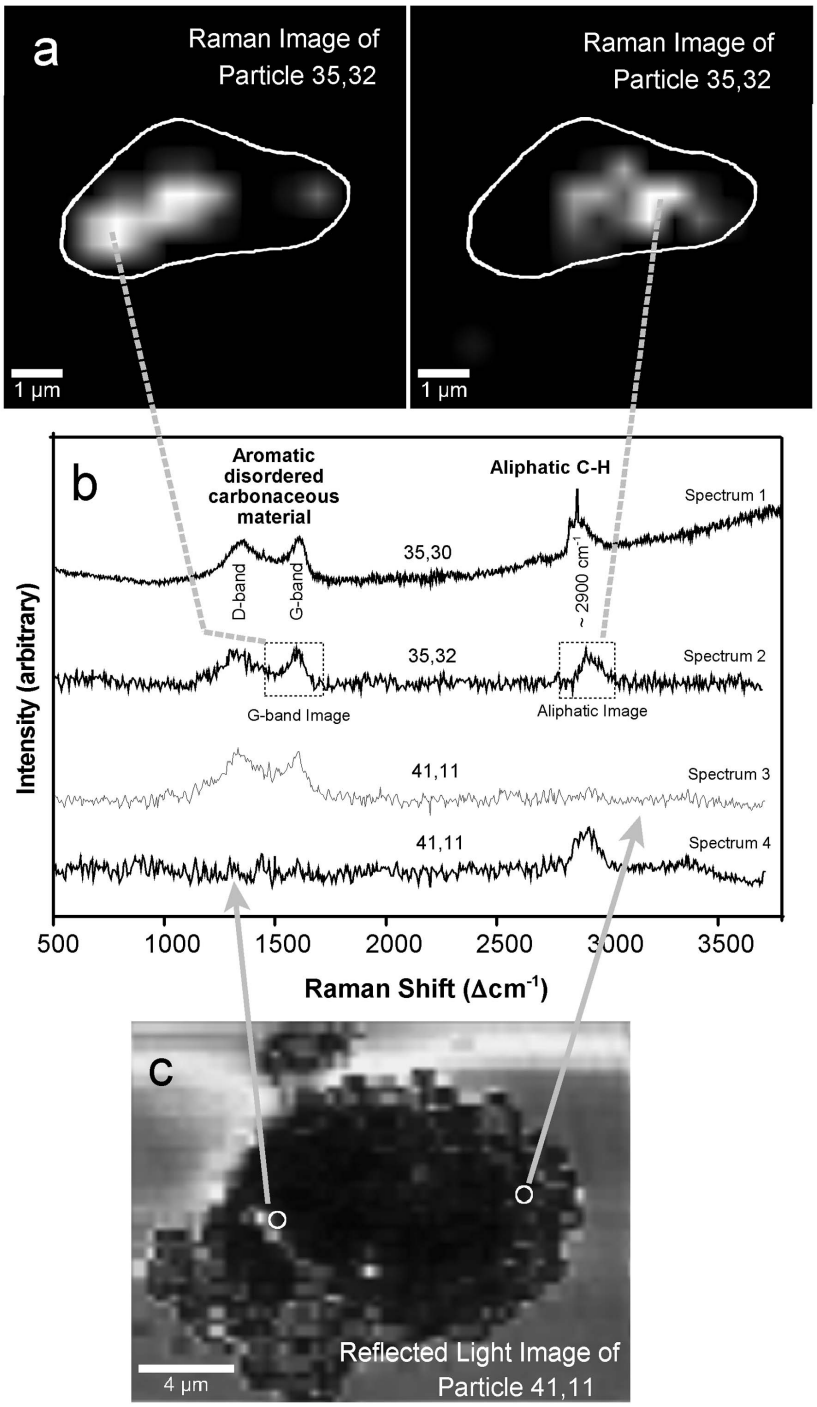

Fig. 6. a) Composite image (360 nm × 360 nm pixels) of Raman band intensities of the microtomed particle 35,32. A full Raman spectrum of each pixel is acquired (see part b), but imaged are only the relative intensities of both the D and G bands (shown on the left-hand side of Fig. 6a) and the C-H band ~2900 Δcm-1 (shown on the right-hand side of Fig. 6a) of each spectrum. Note that spectrum 2 (part b) shows the presence of both components. Overall, however, the Raman images in Fig. 6a show that most pixels in this particle are either dominated by the aromatic sp^2-bonded carbon phase or the aliphatic hydrocarbon phase. Thus, the aromatic and aliphatic components in this particle are mostly present in spatially separated areas (i.e., as discrete phases) rather than as homogeneously intermixed nanophases. b) Examples of background-corrected Raman spectra obtained on three different particles showing the presence of both disordered carbonaceous material and aliphatic hydrocarbons. Spectrum 1 is from a ~1 μm diameter spot of particle 35,30; spectra 2, 3 and 4 are from individual image pixels from particles 35,32 and 41,11. Note that the observed channel-to-channel fluctuations are dominated by optical interference effects in the instrument, not by counting statistics. c) Visible reflected light image of particle 41,11 that was pressed into a gold foil. The spectra obtained from two selected pixels are shown in Fig. 6b.

resolved peaks in the C-H stretch region, but rather a single broad unresolved peak, whose exact peak position was different for the two particles. The peak position was especially high (2917 Δcm^{-1}) in particle 35,32 which was mounted on the amorphous SiO_2/SiO membrane as substrate. The Raman image obtained from this particle (Fig. 6a) indicates that the aromatic C-C bonded phase (e.g., material exhibiting D and G bands) of the disordered carbonaceous material (shown on the left-hand side of Fig. 6a) is spatially separated from the phase whose spectrum is dominated by the aliphatic C-H stretching vibrations (shown on the right-hand side of Fig. 6a). However, in this particle we also found areas where these two phases were found in the same spectrum, i.e., within the spatial resolution limit of $(360\ nm)^2$ (see spectrum 2 in Fig. 6b).

In the case of particle 41,11 the aliphatic peak position was found at 2909 Δcm^{-1}, and the aliphatics were discovered to be intimately intermixed with the disordered aromatic carbon phase exhibiting the D and G bands. Indeed the aliphatics seem to pervade the interior of this particle (Fig. 6c), which argues against post-capture contamination. Given that this particle, as well as particle 35,30 were pressed in gold, a contamination from the mounting medium can be excluded for those two particles. However, this leaves open the possibility that the aliphatic bands seen in these two particles are caused by the limited amounts of organics that are present in aerogel. Of interest, however, is that the C-H peak positions are different for the two particles, which indicates heterogeneity in alkane saturation and/or aliphatic functionalization. Specifically, the apparent absence of $=CH_3$- stretch modes in particle 41,11 argues for either a cross-linked or a very functionalized aliphatic phase.

Fundamentally, the two most likely sources for Stardust aliphatic materials are either native cometary materials and/or minor contaminants introduced during capture and/or curation. Aliphatic hydrocarbons are common terrestrial contaminants for extraterrestrial samples (e.g., Sephton et al. 2001). It is currently unclear whether the minor hydrocarbon contaminants in the aerogel can cause the observed C-H Raman bands or whether contaminants exist in sufficient quantity to generate a condensed phase upon post-capture cooling. Curatorial procedures specifically limited exposure of Stardust particles to organic and polymeric contaminants, and neither particle 35,30 nor particle 41,11 were mounted in epoxy. In addition, contamination is an unlikely source for the aliphatic compounds because different C-H Raman mode structures were observed in those two particles.

In summary, three particles showed peaks in the 2900 Δcm^{-1} region characteristic of aliphatic hydrocarbons. At the moment, these aliphatic materials cannot be ruled out as contamination and this issue needs further investigation beyond the PE phase of the Stardust Mission. Studying the trend of the aliphatics content versus sample surface area could in principle help diagnose whether contamination is important (Sephton 2002), but it is not in fact possible to derive this information for these samples due to the irregular layer with high porosity of aerogel present on the grains surface.

Combined Micro-IR Spectroscopy and FESEM-EDX

For eight particles, six extracted from Track 35 and two extracted from Track 41, a combined FESEM/EDX, micro-FTIR, and micro-Raman analysis was performed (see Table 1). The Raman data for these eight particles have been described in the previous section. For particles 35,21 and 35,26, studied by the IAS team, FESEM/EDX analysis was applied as an initial survey, whereas the other six, studied by the LANDS team, micro-IR and micro-Raman spectroscopy were performed before FESEM/EDX analyses. In all cases, both the FESEM imaging and the EDX mapping results indicate the presence of a considerable amount of aerogel mixed with the particle (Fig. 7). In particular, Si/Mg and Si/Fe were always found to be much higher than what is expected for normal silicate minerals and were seen in some cases to reach values as high as 10. These results confirm the general observations made during PE of compressed or melted aerogel surrounding the particles (Zolensky et al. 2006). Any interpretation of data from Stardust particles will have to take this fact into account. In particular, for the interpretation of the IR data, great care must be taken in the subtraction of the IR spectrum of the aerogel.

To assess the contribution of aerogel to infrared measurements of Stardust samples, aerogel slices were sectioned in the cells from which the grains analyzed here were extracted. FTIR spectra of aerogel slices C2054,32,0,0,0 and C2054,31,0,0,0, near the tracks containing some of the analyzed particles, were acquired by the IAS and LANDS teams in 4000−600 cm^{-1} range at 2 cm^{-1} resolution and normalized to background KBr spectra (Figs. 8−12). Aerogel spectra are dominated by a well-defined band at 1086 cm^{-1} with a shoulder at 1204 cm^{-1}, due to its SiO_2 composition. Further features observed in aerogel spectra are attributed to adsorbed H_2O molecules (3745 cm^{-1} OH dangling bonds, 3400 cm^{-1} OH stretching, 1670 cm^{-1} OH bending, and 809 cm^{-1} OH libration) and to CH aliphatic bonds (2970, 2939, 2881, 2858 cm^{-1} CH stretching, 1464 and 1373 cm^{-1} CH bending).

All the spectra of the analyzed particles were corrected for aerogel contribution with the exception of particle 35,17 for which the subtraction of the aerogel spectrum was not necessary (Fig. 11). We note that the profiles of the aerogel features are significantly different from those observed in aerogel-contaminated cometary particles spectra. After subtraction of the aerogel contribution from that of the cometary particles, spectra were obtained with a richness of signatures that was not detected in the pure aerogel. Thus, the spectra could be assigned to compounds originally present in the particles (although these materials may have undergone varying amounts of alteration or re-distribution due to impact processing).

The infrared CH stretching features in the 3050−2750 cm^{-1}

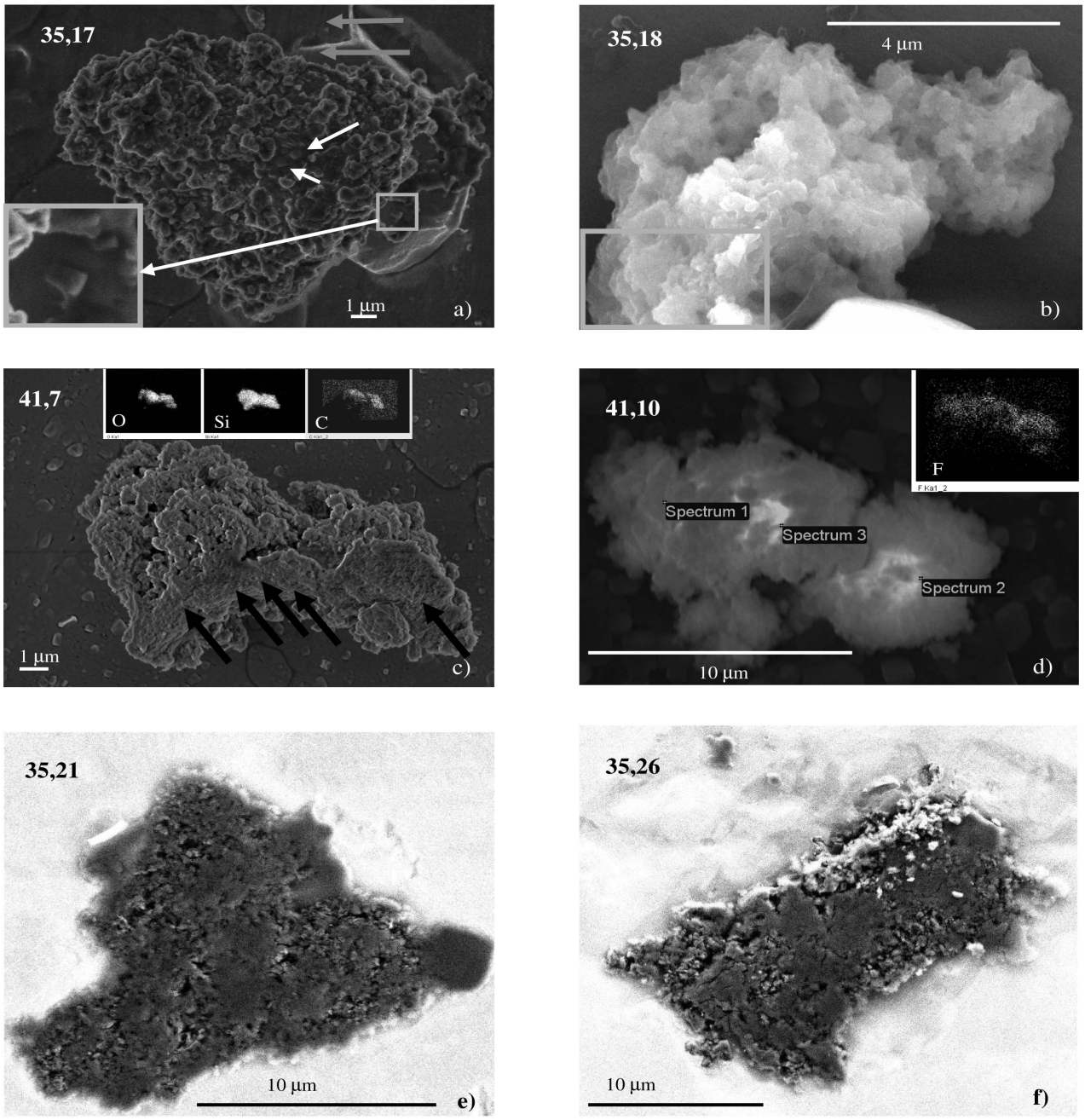

Fig. 7. FESEM images of Stardust particles: a) 35,17 showing porous structure that could be crushed and melted aerogel produced by the entrance of the particle. Some tiny, possibly crystalline grains are present on the porous surface (white arrows) of the grain; the zoomed-in area is 8 µm × 0.5 µm. Gray arrows show straight tracks present on the substrate and continuing on the crystal lying underneath the grain which is a KBr crystal grown-up from the substrate; b) The composition of particle 35,18 is relatively homogeneous with the exception of C that was detected in amount of about 20 atomic% in one specific area indicated by the black rectangular; c) Particle 41,7 appears very porous and fluffy and may be covered by aerogel particularly in the area indicated by the black arrows; d) Particle 41,10 appears very porous and fluffy and may be covered by aerogel. Three areas where the EDS analyses were performed are labeled as spectrum 1, 2 and 3; e) particles 35,21 and f) 35,26 imaged at the same magnification. Both particles are pressed into a gold substrate. Each pressed grain has a size of ~20 µm. The darkness of the grain, relative to the gold substrate is because of the presence of aerogel mixed with the grain.

(3.28–3.64 µm) region are different in the particles compared to the features produced by aerogel alone. In Fig. 12a, the spectrum of a piece of aerogel extracted close to Track 35 is compared with the spectra obtained from the aerogel contaminated particles from this track and the differences are marked, suggesting that most if not all spectral features obtained from the four particles are intrinsic to the particles and not due to the aerogel. A similar trend is noted for additional

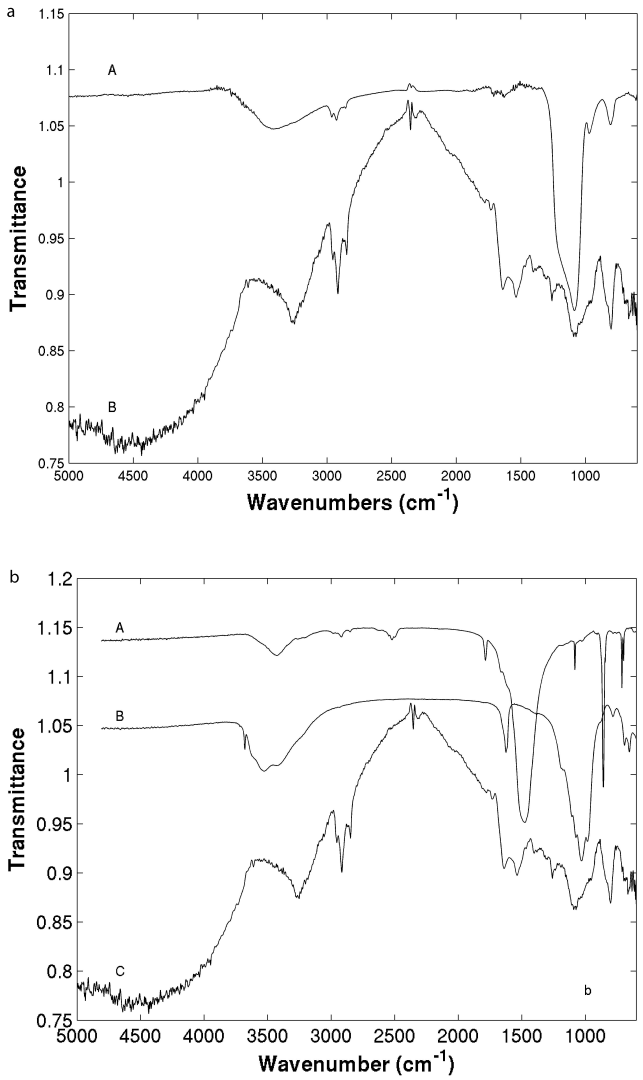

Fig. 8. a) Micro-infrared spectra of (A) aerogel #C2054,32,0,0,0 and (B) particle 35,17. The spectrum of the Stardust particle is modulated by interference of infrared light with a minimum at 4500 cm^{-1} and a maximum at 2330 cm^{-1}. Spikes observed at 2330 cm^{-1} are due to missed compensation for telluric CO_2;. b) Micro-infrared transmittance spectrum of (A) aragonite ($CaCO_3$ polymorph) and of (B) sepiolite (Hydrated sheet silicate) compared with spectra of (C) particle 35,17. The spectra of the minerals were vertically shifted for sake of clarity.

track analyses reported by Sandford et al. (2006) and Bajt et al. (Forthcoming), which yielded clear differences between the IR spectra of material in and near some tracks and aerogel distant from the tracks.

Major differences in abundances of heavy elements are seen in particles from track to track and for individual particles within a single track (Flynn et al. 2006), suggesting similar differences may be seen in the infrared data. To underline the differences observed in the characterization of particles originating from the same track, and thus the same incident particle or between tracks from different aerogel cells, we will discuss the results for four particles from Track 35 (particles 17 and 18, observed in the transmission mode and particles 21 and 26 observed in the reflection mode), and two particles from Track 41 (particles 7 and 10).

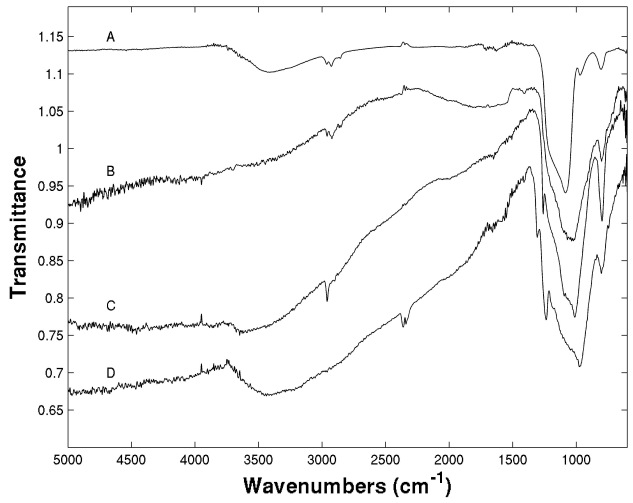

Fig. 9. Transmittance spectra of (A) aerogel #C2054,32,0,0,0; (B) particle 35,18; (C) particle 41,7; (D) particle 41,10. The spectra are not corrected for aerogel contribution and are shifted vertically for sake of clarity.

IR/FESEM_EDX Analyses of Particles from Track 35

Particle 35,17 is the most distinctive in this study, based on optical microscopy, FESEM/EDX, and IR micro-spectroscopy observations. In addition, the micro-Raman spectra of this particle show that the carbon component in this sample is among the most disordered and primitive ones (Fig. 3a). This particle has a yellowish appearance in the reflected light optical microscope. FESEM analyses (Fig. 7a) exhibit a morphology that recalls the aerogel porosity after impact of a hypervelocity circum-terrestrial particle on collectors exposed outside the MIR station (Ferrini et al. 2001). On the porous surface, some tiny, possibly crystalline, particles are present (white arrows in Fig. 7a) that were not observed on the other samples. The large crystal lying under the right side of the particle is actually a KBr crystal, part of the substrate probably accreted under the particle (Fig. 7a). This can be deduced from the straight tracks present on the substrate continuing on the crystal (grey arrow) and by the shape of the tear edges of the thin layer present on the crystal and on the substrate, i.e., the KBr Cr coating, (see the Experimental section). The elemental analysis of this particle, reported in Table 3, shows an atomic ratio Si/O = 0.08, which is low compared to values of 0.25−0.5 expected for silicates, as well as for a possible aerogel contamination. The EDX spectra acquired in different areas of the particle reveal relatively homogeneous elemental composition with the exception of C that was detected to range from 1 wt% to 10 wt% in different areas. The infrared spectrum (Fig. 8), in which the main aerogel features at

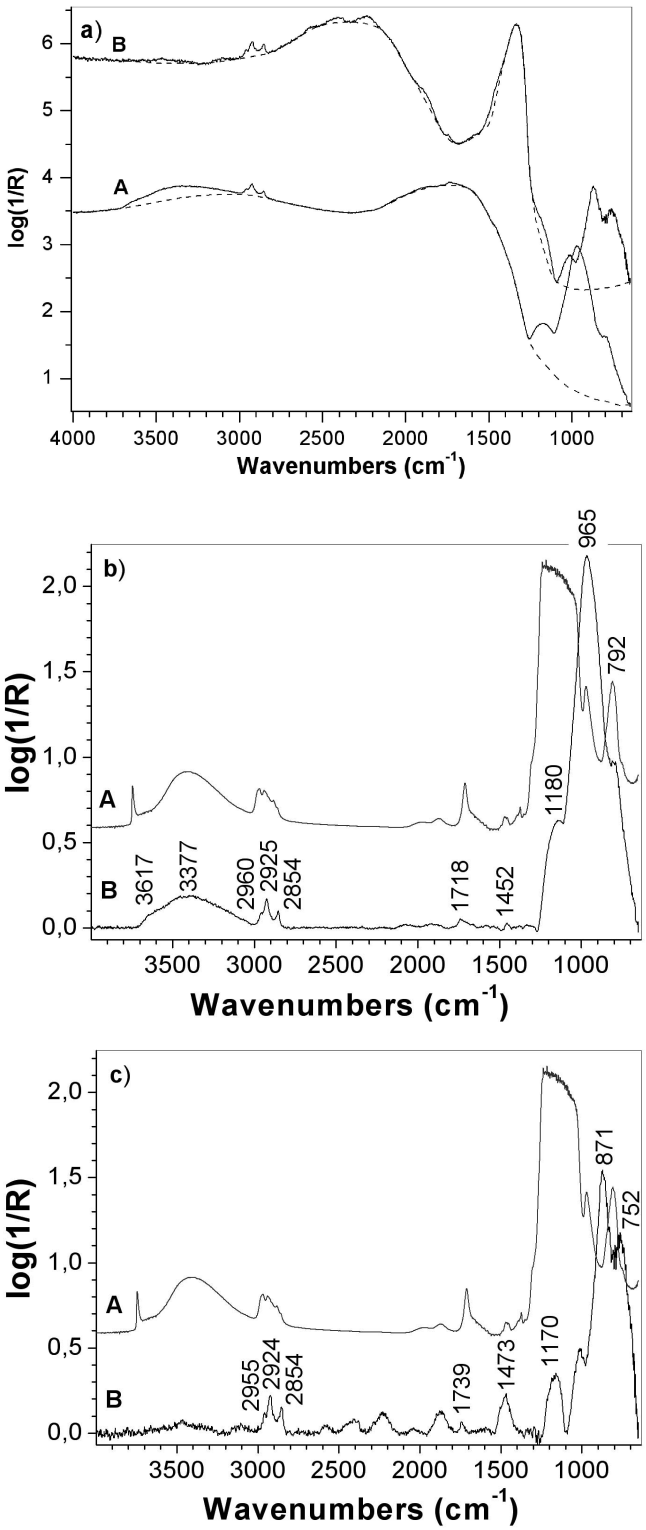

Fig. 10. a) Mid IR reflectance spectra of particles 35,21 (A) and 35,26 (B) before the baseline correction. The baselines adopted are in dashed lines. The spectra are shown in the adsorption mode. (b) Mid IR spectra in absorption mode of a piece of aerogel (A) and of particle 35,21 (B) after the baseline correction c) Mid IR spectra in absorption mode of a piece of aerogel (A) and of particle 35,26 (B) after the baseline correction.

1086 cm^{-1} and 1204 cm^{-1} are negligible, indicates that the amount of aerogel associated with this particle is low. This spectrum is complex: it shows several features superimposed on a continuum modulated by interference of infrared light passing through the particle. Interference phenomena become more pronounced when the size parameter $x = 2\pi a/\lambda$, where a is the particle radius and λ the wavelength, is similar to the wavelength of light. This particle has a diameter of about 13.5 μm, which corresponds in our spectral range to a size parameter >2.5, responsible for a broad continuum variation with a minimum at 4500 cm^{-1} and maximum at 2330 cm^{-1}, where the incomplete compensation for telluric CO_2 generates the narrow "spikes" near 2350 cm^{-1}. The peaks near 3250, 1640, and 800 cm^{-1} are characteristic of H_2O molecules. Aerogel is very hygroscopic, thus water adsorbed by the aerogel during particle capturing or adsorbed from the laboratory environment could account for the presence of the H_2O stretching, bending, and libration modes. Nevertheless, we note that among the six particles analyzed by FESEM/EDX and micro-IR spectroscopy, particle 35,17 appears to be the least contaminated by aerogel. The IR spectrum of the particle shows the OH stretching band to be more intense and narrower with respect to that present in the aerogel spectrum and also shows a very weak SiO stretching band (Fig. 8a). The shape of the feature at 3400 m^{-1} observed in the aerogel slice C2054, 32,0,0,0 (Fig. 8) is broader and peaked at larger wavelength with respect to this particle. This could be an indication that a fraction of H_2O molecules are present in the mineralogical structure of hydrated silicates. These IR observations are consistent with the results of the EDX analysis, as the low Si/O (the lowest among the analyzed particles, see Table 3) supports the presence of H_2O observed in the IR spectrum that is responsible for the high amount of oxygen detected. The combination of the micro-IR and EDX data suggests that particle 35,17 might contain phyllosilicates containing Ca, Al, Na. In fact, many hydrated silicates are characterized by bands peaked at about 1020 cm^{-1} due to SiO stretching mode (broad and intense), 1630 cm^{-1} due to H_2O bending mode, and around 3550 cm^{-1} due to hydroxyl stretching mode (broad). For example, Montmorillonite $[(Na,Ca)_{0.3}(Al,Mg)_2Si_4O_{10}(OH)_2.nH_2O]$ and sepiolite $Mg_4Si_6O_{15}(OH)_2.6H_2O$ spectra show features matching those present in the 35,17 spectrum (Fig. 8). The bands at 1026, 914, and 843 cm^{-1} of montmorillonite may appear as the shoulders at 1028, 918, and 839 cm^{-1} in the spectrum of this particle and the bending mode of H_2O is responsible for the feature at 1638 cm^{-1}. The clay sepiolite $Mg_4Si_6O_{15}(OH)_2 6H_2O$ shows intense peaks at 1030 and 1626 cm^{-1} due to SiO stretching and H_2O bending mode, respectively, and two characteristic peaks at 690 and 656 cm^{-1} are also present in this Stardust particle.

On the other hand, the IR spectrum of particle 35,17 exhibits bands at 1450 cm^{-1}, 860 cm^{-1}, as a shoulder, and two twin peaks at 700 and 714 cm^{-1}. Recalling that the main characteristic bands of carbonates are centered at about 3420,

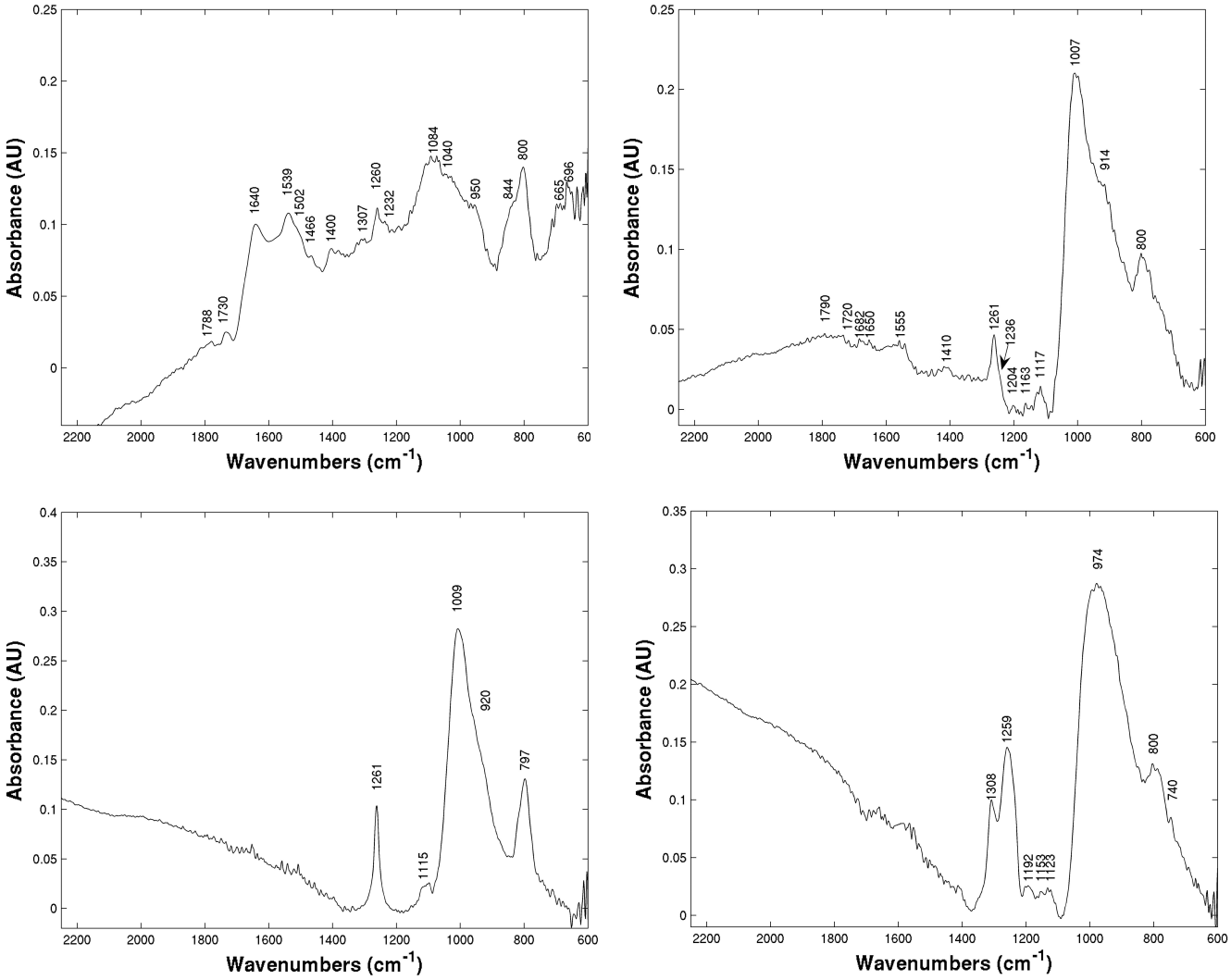

Fig. 11.IR spectra of particle 35,17 (up left); 35,18 (up right); 41,7 (bottom left) and 41,10 (bottom right) in the 600–2250 cm^{-1} range. All the spectra are corrected for aerogel contribution with the exception of particle 35,17 for which the subtraction procedure was not necessary because of the negligible aerogel contribution.

1450, 860, and 730 cm^{-1} and that Ca and C are detected by EDX in this particle we infer the presence of carbonates in this particle. This is supported by the comparison of the aragonite ($CaCO_3$) spectrum (Salisbury et al. 1991) with that of particle 35,17 (Fig. 8b).

Supporting data from techniques like X-ray diffraction and Transmission Electron Microscopy (TEM) that would unambiguously determine the mineralogy are essential to corroborate the interpretation of the spectral features described above in terms of phyllosilicates and carbonates.

EDX analyses of particle 35,17 detected potassium and bromine, these elements can be interpreted as a contribution from the substrate, i.e., a KBr window (K/Br = 1 atomic%). However, an excess of K with respect to Br is measured (K/Br = 4.4 atomic%) while we would rather expect an excess in Br if the presence of these elements was really exclusively due to the substrate. This is what we find for particles 41,7 and 41,10 for which we measure a K/Br ratio of about 0.5 atomic% explicable as an artifact. In fact, the particle, lying over the substrate, shields the signal coming from the substrate with a selective X-rays absorption due to the different atomic number. Thus we can conclude that the K excess is indigenous to particles 35,17.

Particle 35,18 is about 10 mm in size and has a very dark appearance in the reflected light optical microscope. As in the case of particle 35,17, the morphology of this particle (Fig. 7b) is similar to that seen in aerogel after impact of an hypervelocity circumterrestrial particle (Ferrini et al. 2001). The IR spectrum of the particle shows a common feature at 1028 cm^{-1} due to SiO stretching mode and bands at 3400, 1600 (noisy), and 802 cm^{-1} due to H_2O (Fig. 9). The detection of minerals is difficult, because the SiO stretching mode feature, probably due to the aerogel, is very intense (Fig. 9). The IR spectrum, corrected for aerogel contribution, does not show the

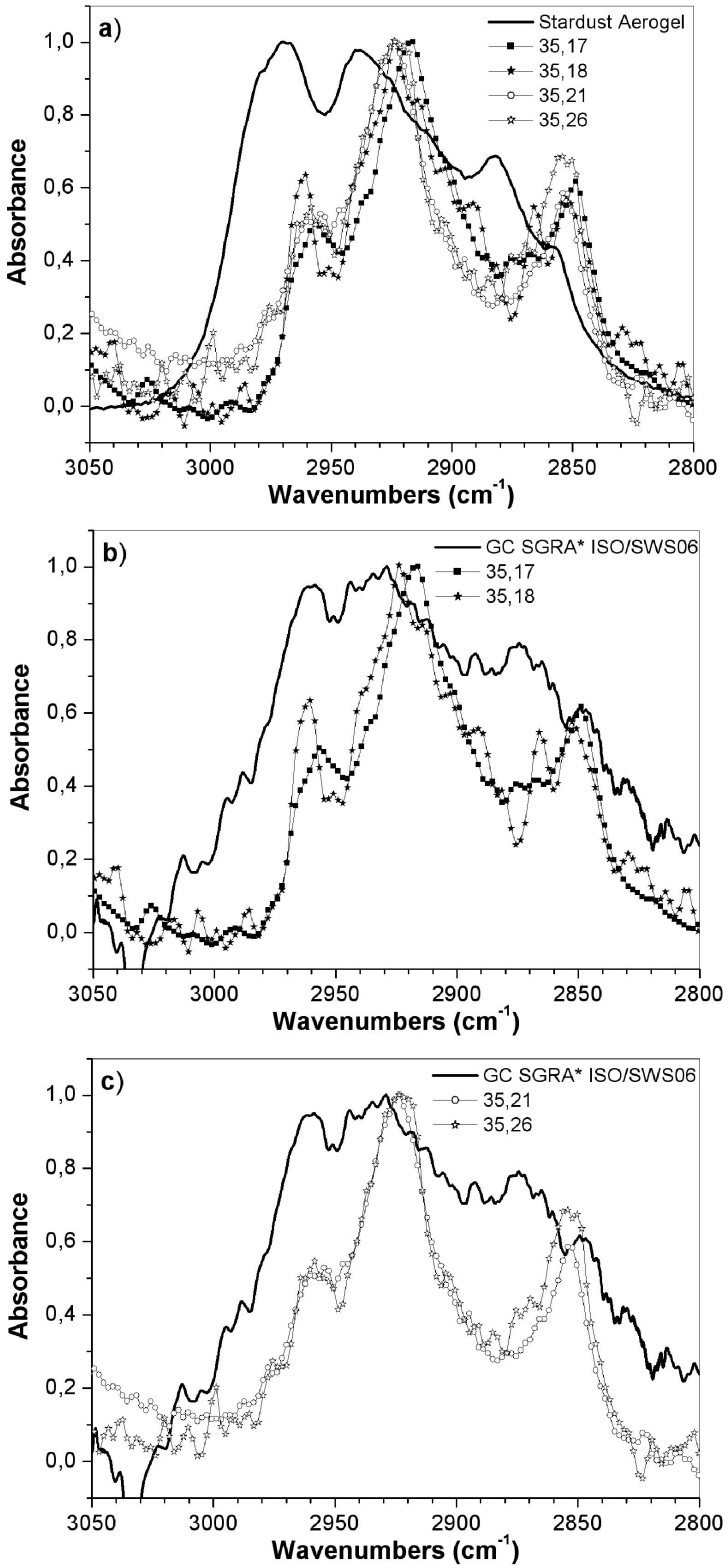

Fig. 12. a) Comparison of the infrared CH stretching features of Stardust aerogel (cell # C2054,31,0,0,0) with those of 4 stardust grains extracted from Track 35 in the same cell. The curves have been normalized so that the main peak in aerogel (2974 cm^{-1}) is normalized to the depth of the main peak of the CH_2 contribution near 2945 cm^{-1} in all four particles. The profile of the CH stretching feature of the particles is clearly different from that of the aerogel in which they were captured. b) Comparison of the CH stretching features of the Galactic Center Source SGRA (ISOArchive) and those of 4 Stardust grains: 35,18; 35,17; 35,21; 35,26. The Stardust grain spectra are not subtracted from the aerogel contribution because in this region the features present in the aerogel spectrum appear completely different from those present in the particles spectra.

Table 3. Elemental abundances for the four particles analyzed by FESEM/EDS. Average values are reported for particles 35,17; 35,18;, and 41,7 since the composition does not vary significantly from location to location. For particle 41,10 elemental abundance for three different spectra are reported since the particle showed a high compositional heterogeneity.

Particle#	35,17	35,18	41,7	41,10		
				Spectr. 1	Spectr. 2	Spectr. 3
Element	at%	at%	at%	at%	at%	at%
C	13.30	*	14.64	2.99	n.d.	n.d.
O	57.96	66.19	61.21	57.49	56.71	29.99
Na	2.33	2.15	0.23	n.d.	n.d.	n.d.
F	n.d.	n.d.	n.d.	17.90	9.66	n.d.
Mg	0.28	0.87	0.48	0.33	0.52	n.d.
Al	3.50	n.d.	n.d.	n.d.	n.d.	n.d.
Si	7.65	10.93	19.20	16.63	20.40	n.d.
Cl	0.26	0.24	n.d.	n.d.	n.d.	n.d.
S	n.d.	n.d.	0.53	0.10	0.27	n.d.
K	10.66	11.38	0.99	1.81	2.84	15.67
Ca	0.86	n.d.	n.d.	n.d.	n.d.	n.d.
Cr	0.09	1.21	0.11	n.d.	n.d.	n.d.
Fe	0.52	0.99	0.52	0.10	0.30	n.d.
Ni	n.d.	n.d.	0.12	n.d.	n.d.	n.d.
Cu	0.17	0.31	0.15	0.22	4.64	23.50
Br	2.43	4.75	1.81	2.44	4.65	30.84
Ag	n.d.	0.16	n.d.	n.d.	n.d.	n.d.
Total	100.0	100.0		100.0	100.0	100.0

*For particle 35,18 the composition is quite homogeneous except for C which was detected in amount of about 20 at% only in one specific area.

wide smooth band of amorphous silicate usually extending in the 1300−800 cm^{-1} range with a peak at about 1020 cm^{-1}. Characteristic crystalline silicate peaks are not observed in the spectrum. All spectral features that remain after correction for the aerogel contribution are from C-based materials (see Organics section). C was detected by EDX analyses in the amount of about 20 atomic% in one specific area. In this particle, as in particle 35,17 the potassium content is higher than bromide (K/Br = 2.4 atomic%) suggesting an indigenous presence of K in this cometary particle.

Particles 35,21 and 35,26 were pressed in gold and their infrared spectra were obtained in the reflection mode. FESEM imaging reveals similar features for both particles, as shown in Figs. 7e and 7f. They appear dark under the beam, which is characteristic of light elements. The lateral sizes of the particles after pressing are around 20 μm. The overabundance of the light elements is confirmed by the EDX spectra of the two particles. The spectra are dominated by Si (Mg/Si about 0.1 for both particles) and O, whereas Mg and Fe—which are supposed to be the dominant cations in silicates—are under represented by at least a factor of 10, suggesting that residual aerogel is present in these samples.

Figure 10a shows the raw spectra in the mid IR region (4000−600 cm^{-1}) for the two particles. The IR beam reflects on the gold foil, resulting in the IR photons making two passages through the particles. Hence log(1/R) is equivalent to absorbance. The typical propagation length of the IR beam inside the particles can be estimated: a typical particle that has been flattened to ~17 μm size exhibits a thickness in the 3−4 μm range and, therefore, the propagation length of the IR light inside the particle is of the order of the wavelength. This leads to complex scattering effects affecting the absorption spectrum of the sample (Raynal et al. 2000). Mainly the <2000 cm^{-1} (>5 mm) region is affected. For instance, the bands at 1750 cm^{-1} for 35,21 and at 2300 and 1330 cm^{-1} for 35,26 are interpreted as optical scattering effects predicted by Mie theory (Bohren and Huffman 1983). No precise refractive index can be calculated because of the complex composition of the particles. Therefore, the baselines (dotted lines in Fig. 10) were empirically chosen to exclude the broadest lines. Figs. 10b and 10c show the corrected spectra and the spectrum of a piece of aerogel (C2054,31,0,0,0), respectively, as well as assigned band positions in the 3600−600 cm^{-1} region. The 4000−2700 cm^{-1} region will be discussed in the next section on organic features. The interpretation is arduous, because of the optical effects and the presence of aerogel. However, we can identify some signatures of silicates in the 1000 cm^{-1} region. In particle 35,21 (Fig. 10b) we observe a mixture of amorphous and crystalline silicates and a characteristic OH signature, marked by the presence of a broad band at 3377 cm^{-1} and accompanied by a weak feature at 3617 cm^{-1}. This is characteristic of isolated OH, as it is seen in phyllosilicates. For particle 35,26 (Fig. 10c) we cannot rule out that OH features are from the aerogel. In contrast to particle 35,21, particle 35,26 is mainly composed of crystalline olivine (bands at 1017 and 871 cm^{-1}) and hydration is not evident. IR

spectra of two particles from Track 35 indicate the presence of hydrated minerals, and we hypothesize that hydrated minerals (phyllosilicates) and carbonates could both be present. However, unambiguous evidence for such phases has not yet been found by transmission electron microscopy or X-ray diffraction studies of Stardust samples (Zolensky et al. 2006).

IR/FESEM_EDX Analyses of Particles from Track 41

Particle 41,7 (15.5 μm × 5.5 μm) appears very porous in the FESEM image except for the bottom part (see black arrows in Fig. 7c) where the surface is smoother. The morphology suggests the particle is uniformly covered with aerogel. This is supported by the EDX maps, which show a uniform distribution of Si and O over the particle surface (Fig. 7c) and the lack of any useful C Raman spectra (see Table 2). The absence of the O signal in the bottom left part of the map is an artifact, because the detector (upper right) is shadowed by the particle. Carbon is distributed throughout the particle, but is particularly concentrated in the two areas in the bottom right and upper left, but neither seems to be Raman active. After correction for aerogel, the IR spectrum (Fig. 11) does not show any signature of silicates in the 2250–600 cm^{-1} range, while the bands related to organic molecules become evident (see the Organics section below).

Particle 41,10 (size 10 μm × 16 μm) appears very porous and fluffy in the FESEM (Fig. 7d). It appears uniformly covered by aerogel, as deduced from both its morphology and EDX maps, which show a relatively uniform distribution of Si and O on the particle surface. The other elements show large variations (Table 3). The area where spectrum 3 was acquired (see Fig. 7d) is particularly rich in Cu and poor in O, and F is not detected while it is abundant in the rest of the particle (see Fig. 7d). The IR spectrum of this particle (Fig. 9) shows many bands also found in particle 41,7, although small variations in band positions are observed. In fact, micro-infrared spectra of both particles show common features at 1028 cm^{-1} due to SiO stretching mode and bands at 3400, 1600 (noisy), and 802 cm^{-1} due to H_2O (Fig. 9). The detection of minerals is difficult, because the SiO stretching mode feature of the aerogel is very intense in this sample.

Organic IR Features in Stardust Particles

Hydrocarbons are rich in vibrational modes with bending frequencies that are observed in the 2000–600 cm^{-1} spectral region. A detailed analysis of this region for particle 35,17 reveals the presence of a large number of features (Fig. 11). Peaks are seen at 1788, 1730, 1640, 1539, 1502, 1466, 1400, 1307, 1260, 1084, 950, 844, 800, and 665 cm^{-1}. Peaks at these positions are compatible with the presence of a multitude of polycyclic aromatic hydrocarbon (PAH) species, i.e., molecules that contain 5 and 6 membered aromatic rings in a wide variety of configurations (e.g., Szczepanski and Vala 1993; Hudgins and Sandford 1998a, 1998b, 1998c; Langhoff et al. 1998). The number of features and the peak positions are consistent with the presence of small aromatic molecules in particle 35,17. This result is consistent with the μL^2MS detection of low-mass polycyclic aromatic hydrocarbons (PAHs) in aerogel tracks (Sandford et al. 2006).

Table 4. The calculated CH_2/CH_3 functional group number ratios for the four particles, extracted from Track 35 that showed the CH stretching band in their IR spectra. For the ratios calculation, the aerogel contribution was neglected because in this region the features present in the aerogel spectrum were different from those of the particles spectra.

Particle #	35,17	35,18	35,21	35,26
CH_2/CH_3	6.1 ± 1.0	9.6 ± 2.5	5.9 ± 1.2	5.7 ± 1.5

Particle 35,18 and particle 41,7 (Fig. 11) also show spectra with the CH_3 bending mode at 1261 cm^{-1}. There has been an effort to identify some features related to the eventual presence of N in some grains. For particle 35,18 the peak at 1410 cm^{-1} could be related to aromatic carbon stretching mode or to the NHO functional group. Nitrile (–C≡N) functional groups, which typically show peaks in the 2245–2162 cm^{-1} frequency range (e.g., Bernstein et al. 1997), are not observed in any grain analyzed. However, the intense peak at 1007 cm^{-1} observable in the silicate region could be related to chemical links between carbon atoms of organic molecules and silicon or to single bond C-N in methenamine (hexamethylenetetramine) that also shows features near 1370 (–CH scissoring), 1240 (C-N stretching), and 820 (NH_2 wag) cm^{-1}, (Bernstein et al. 1994), which are observed in Fig. 11 as weak shoulders. Hence, this suggests the possible presence of aliphatic amine groups in particle 35,18. In particle 41,7 the peak at 1115 cm^{-1} may be due to HNC or NH_3 bending modes. As observed in particle 35,18 the peak at 1009 cm^{-1} could be related to chemical links between the carbon atoms of organic molecules and silicon. However, if the methenamine C-N bond is responsible for this intense peak, the shoulder at larger wave numbers of the band at 797 cm^{-1} could be related to NH_2 scissoring feature expected at 820 cm^{-1}. Note that the peaks at 1236 cm^{-1} (CN stretching) and 1375 cm^{-1} (–CH scissoring) possibly due to methenamine observed in 35,18 are not detected in this particle or are very weak with respect to the S/N ratio.

Particle 41,10 contains bands in the 1400–1100 cm^{-1} whose positions might be consistent with the presence of aromatic hydrocarbons (Fig. 11), although their relative strengths are not those typical of PAHs. This peculiarity is attended with an absence of measurable CH aliphatic and aromatic stretching features in the 3100–2750 cm^{-1} region. The source of these bands is therefore unclear.

For the two grains analyzed in the reflection mode (35,21 and 35,26), the detection of small features in the 2700–600 cm^{-1} region is much more arduous, because of the interference pattern resulting from the dual passage of the IR beam through the grain (Fig 10). It is with great caution

that we identify in grain 35,26 a very weak C=O stretch mode at 1739 cm^{-1} and a CH_3 asymmetric mode at 1473 cm^{-1}. The 2232 cm^{-1} C≡N nitrile feature is consistent with the detection of N in this grain by NanoSIMS investigation (Sandford et al. 2006); unfortunately the use of the Cs^+ beam needed for this analysis has made all future analyses impossible. For the grain 35,21, there is a possible C=O stretch feature at 1718 cm^{-1} and a CH_3 asymmetric deformation at 1452 cm^{-1}; no N has been identified.

All the particles extracted from Track 35 and examined by micro-IR spectroscopy (i.e., particles 17, 18, 21, and 26, Fig. 12a) show CH stretching bands near 2960 cm^{-1} (from asymmetric stretching of CH_3 groups), near 2920 cm^{-1} (from asymmetric stretching of CH_2 groups), and near 2855 cm^{-1} (from blended symmetric CH_2 and CH_3 groups). These features, corresponding to aliphatic hydrocarbons, all fall at positions that vary slightly depending on the specific molecular structure. In particle 35,17, a band at 3058 cm^{-1}, assigned to CH stretching in aromatic hydrocarbons, is also observed. Particles from Track 41 (i.e., Particles 7 and 10) do not show the same complete CH stretching band features (Figs. 9c, 9d). Particle 41,7 shows only the CH_3 asymmetric and symmetric stretching modes at 2961 and 2901 cm^{-1}, respectively. In contrast, the CH stretching features due to aliphatic hydrocarbons, and aromatic CH stretching features are absent in the IR spectrum of particle 41,10.

For each of these particles, we calculated the $-CH_2/-CH_3$ ratios converting the band areas to column densities, following Matrajt et al. (2005):

$$\frac{CH_2}{CH_3} = \frac{\left(\int \frac{\tau_\upsilon d\upsilon}{A}\right)_{CH_2}}{\left(\int \frac{\tau_\upsilon d\upsilon}{A}\right)_{CH_3}} = \frac{A(CH_3)}{A(CH_2)} \times \frac{(\int \tau_\upsilon d\upsilon)_{CH_2}}{(\int \tau_\upsilon d\upsilon)_{CH_3}} \quad (1)$$

where τ is the optical depth and A(CHx) represent the band strengths given by Dartois et al. (2004a). The fit of the four CH stretching bands was obtained using 4 Gaussians and the CH_2/CH_3 ratios obtained by these calculations are reported in Table 4. The ratios and spectra are very similar for particles 35,17; 35,21, and 35,26 (Fig. 12a). The value for particle 35,18 is higher than that of the other particles, implying some heterogeneity within the impacting particle. This is consistent with heterogeneities being present in the Track 35 impactor, as evidenced by noticeable differences in Raman, IR, and EDX compositional results (see previous sections).

Interpretation of the Micro-FTIR Spectra and FESEM/EDX Data

Micro-FTIR spectra have been obtained for six particles extracted from Track 35 and two from Track 41. Two of these particles (35,21 and 35,26), were analyzed in transmission-reflection mode and their spectra were found to the first order to be dominated by optical effects. These effects, which depend on the relative sizes of the particles to the size of the wavelength, ensure a strong scattering in the 10 micron region as described by Raynal et al. (2001). Moreover, the presence of fused aerogel clearly visible by other techniques (e.g., FESEM), hampers the analysis of the 1000 cm^{-1} (10 μm) region where silicate features are confused with aerogel signatures.

The IR data suggest the possible presence of phyllosilicates and carbonates in two of the six analyzed particles. This is an important finding suggesting cometary aqueous alteration and consistent with the identification of these phases in the ejecta of comet Tempel 1 excavated by the Deep Impact spacecraft (Lisse et al. 2006). Nevertheless, we would like to stress here that the importance of this finding requires confirmation by further investigation on these grains with other techniques such as TEM and X-ray diffraction. In addition, we recall that aerogel is extremely hygroscopic, and phyllosilicate can be made at room temperature based on experimental data (Chizmadia 2007). Contamination may also be an issue for carbonates, as small carbonates believed to have a terrestrial origin have been detected by Wirick et al. (2007) in particles extracted from 4 different Stardust tracks, and small Ca spots in aerogel were reported by different investigators (Leroux et al. 2008).

On the other hand, Mikouchi et al. (2007) claim that the Mg-Fe carbonate (breunerite) detected in one Stardust particle is indigenous to comet 81P/Wild 2. Clearly the abundance of phyllosilicates and carbonates in Wild 2 samples has yet to be resolved.

Potassium was found in excess in particle 35,17 and in particle 35,18 that cannot be explainable purely as a contribution of the substrate (KBr window). This element can be a substitute for other cations in clays and other hydrated silicates as part of the crystal structure. The presence in particle 35,17 of Al (see Table 3) suggests also the presence of K-feldspar as detected by Mikouchi et al. (2007) in one Stardust grain. In addition, it is worth mentioning that roedderite was also identified by Joswiak et al. (2007) in a Stardust terminal particle.

In the ~2950 cm^{-1} (3.4 μm) region, many studies have shown that aerogel shows different band profiles than the particles (Fig. 12a). We are thus confident that the observed CH_2 and CH_3 bands contain significant contributions from material intrinsic to the particles. Before concentrating on the discussion on the CH_2/CH_3 ratio as measured in the stardust samples, it must be noted that two grains (35,21 and 35,26) show IR spectra almost totally free of oxygen, in particular in the 1700 cm^{-1} region where only two very weak peaks around 1730 cm^{-1} are observed. The position of these weak features corresponds to a C=O stretching in a ketone, a good signature of oxidized materials. Remembering that the intrinsic oscillator strength of this feature is at least ten times higher than the C=H one (D'Hendecourt and Allamandola 1986), we

can safely deduce that C=O is not present in these two grains at levels more than ~1% of C=H. This observation, together with the fact that Raman data clearly indicate only little thermal metamorphism of many of our samples, implies that at least some of the organic carbon in these grains has not suffered much from aerogel entry. Such a statement is difficult for the other studied grains because of the strong contribution of aerogel bands in this region. A similar effect has been noted in the hypervelocity capture of materials in aerogel, where materials in keystoned tracks were found to be oxidized at the entrance of the track while remaining in their initial oxidation state within the terminal grain. This effect was noted both for small Allende grains that were fired in aerogel blocks at similar velocities as the Stardust spacecraft's flyby encounter with Wild 2 or from aerogel collectors exposed outside the MIR station to the extraterrestrial population present on low Earth orbits (Borg et al. 2006; Grossemy et al. 2006). Although this oxidation was determined specifically from the state of iron present in the samples, a similar behavior might be expected for any material, mineral or organic, that reacts with the abundant oxygen of the aerogel during impact. However, the degree of heating decreases with depth in the track and the degree of oxidation should correspondingly decrease. In addition, it is clear that the impact process is a highly stochastic one and that fragile materials can often be protected during deceleration by surrounding materials. Thus, while it is clear that organic materials do survive hypervelocity impact into aerogel, it is reasonable to consider the possibility that some degree of oxidation could occur during the impact process, along the track, and decreasing at the end of it, just as recorded for the iron oxidation state in simulation experiments (Grossemy et al. 2006).

The CH_2/CH_3 Ratios in the Wild 2 Particles and Comparison with these Ratios in ISM and IDPs

The C=H stretching features seen in the Wild 2 samples can be compared to those seen in the spectra of organics in the diffuse ISM and in IDPs. The C=H stretching features of aliphatic hydrocarbons have been observed along many lines of sight in the diffuse ISM (Sandford et al. 1991; Pendleton et al. 1994; Whittet et al. 1997; Chiar et al. 2000; Dartois et al. 2004b). In Fig. 12b and c we compare a spectrum in the C=H stretching region of the galactic center SGR AW (ISO Archive), a line of sight that crosses a long path of diffuse matter in our galaxy with the spectra of Wild 2 particles. For the galactic center data, the CH_2/CH_3 ratio is close to 2.2, similar to that seen in the diffuse ISM along many lines of sight in our galaxy (Sandford et al. 1991; Pendleton et al. 1994) and in the diffuse ISM in the external Seyfert galaxies (Dartois et al. 2004a). The observed CH_2/CH_3 ratios are clearly considerably higher in the spectra obtained from the Wild 2 grains described in this work.

In contrast to what is observed in the diffuse ISM, the similarities between the CH_2/CH_3 ratios of IDPs and the Stardust particles are striking. The CH_2/CH_3 ratios for three of our Stardust particles is around 6 (Table 4); this compares to values ranging from 3.4 to 5.5 for IDPs (Matrajt et al. 2005). A similar comparison can also be made for the primitive meteorite Tagish Lake (Matrajt et al. 2004) where a ratio of 7.3 is found for the organic material, and particle 35,18 for which the CH_2/CH_3 ratio is 9.6 ± 2.5.

It must be finally noted that the situation in the diffuse ISM is quite different to that in dense molecular clouds, where the aliphatic features are not nearly as prominent (Allamandola et al. 1992; Brooke et al. 1996, 1999; Chiar et al. 1996) and the number of aliphatic C=H bonds is reduced by at least 55% with respect to the diffuse regions (Muñoz-Caro et al. 2001).

To identify the nature of the carrier of these features, various cosmic analog materials have been studied in the laboratory. This provides a critical means to assess the possible interstellar origin of the organic matter in the cometary material as sampled by Stardust.

The ~2950 cm^{-1} (3.4 μm) structure observed in absorption in many astrophysical objects (Pendleton et al. 1994; Pendleton and Allamandola 2002; Dartois et al. 2004b) has been studied at length using various laboratory simulations that are able to reproduce, with a high degree of accuracy, the observed lines, not only in the ~2950 cm^{-1} region but also at higher wavelengths. For instance, Pendleton and Allamandola (2002) have analyzed the spectrum of diffuse interstellar dust in the 1000–4000 cm^{-1} range and have compared it with the spectra of 13 cosmic analog materials. To constrain the applicability of the candidate materials, in addition to the profile of the ~2950 cm^{-1} region band, further evaluation criteria have been considered, i.e., the optical depth ratio of the C=H stretching feature to: a) the corresponding deformation modes, b) the O-H stretch band at 3333 cm^{-1}, and c) the carbonyl band at 1724 cm^{-1}. The main conclusion is that the organic refractory material in the diffuse interstellar medium is mainly hydrocarbon in nature, with the carbon distributed between the aliphatic and aromatic forms, and with little oxygen and nitrogen. This material is more similar to plasma processed pure hydrocarbon materials than to energetically processed ice residues. Mennella et al. (2002) and Dartois et al. (2004b) have shown that the best match to the features identified in the IR spectra of diffuse ISM organics, around 2950, 1380, and 1460 cm^{-1}, is obtained with hydrogenated amorphous carbon grains and organic matter with a kerogen-like structure, respectively.

On the basis of the results of laboratory simulations of grain processing in space, modeling of carbon dust evolution indicates that hydrogenation of carbon particles by H atoms may be the key mechanism determining the presence of the aliphatic band around 2950 cm^{-1} in the spectrum of diffuse interstellar dust (Mennella et al. 2002). In the diffuse interstellar medium, competition between C-H bond formation and its

destruction by UV photons determines a fast equilibrium (~10^4 yr) with respect to cloud lifetime (3×10^7 yr), suggesting that the bonds responsible for the observed absorption around 2950 cm^{-1} form in situ. When grains enter dense regions during their cycling between diffuse and dense medium, hydrogenation is no longer active, due to the presence of an ice mantle around particles and the activation energy of aliphatic C=H bonds (Mennella 2006). The breakdown of the equilibrium reached in diffuse regions determines a gradual dehydrogenation of carbon grains, which is driven by cosmic rays and the internal UV field and which can explain the absence of the band around 2950 cm^{-1} in the spectrum of dense cloud dust (Mennella et al. 2003). However, processing of ices in dense clouds may ultimately lead, upon warming, to the production of new aliphatic-containing materials (Bernstein et al. 1995).

Since the CH_2/CH_3 ratio is a tracer of the length or branching of the alkane chains in the organic matter, it is easy to deduce from these comparisons and with some confidence, that the organic matter in Stardust samples differs from diffuse interstellar matter; it has been reprocessed to some degree in the dense interstellar medium, in the protosolar nebula, and/or in the cometary parent body at a scale and with physical phenomena which remain to be specified in further studies. In particular, aliphatic chains in IDPs are longer (or less branched) than those in ISM spectra and altogether, the bands in IDPs and Stardust samples are less broad and more pronounced than those observed in the ISM. Organics in IDPs, like in Stardust particles, contain components that are less aromatic and more aliphatic than the kerogen in the ISM, thus less mature in the sense of Van Krevelen (Durand 1980). This result is highly surprising as carbon maturity (from aliphatics to aromatics) irreversibly goes down a thermodynamic ladder from less mature (aliphatic) to more mature (or graphitic) in the Van Krevelen diagram (Durand 1980). The organic carbon, observed in some of the Stardust grains, but also in other primitive samples like some IDPs, must have a different origin since it cannot simply derive from a thermal reprocessing. Another possibility is that this material could be the result of reprocessing of the initial molecular cloud phase organics within the primitive solar nebula where different physico-chemical conditions are encountered. Since this phase has remained unoxidized, as revealed by the almost complete absence of ketones and alcohols in the analyzed samples, we may assume that reactions in the solar nebula must have taken place in a rather reducing environment (H_2/CO) rather than an oxidizing one (H_2/CO_2). Further laboratory simulations are strongly needed to quantitatively investigate these processes, not only from a chemical point of view but also from a kinetic one (i.e., involving time scales in the nebula).

Clearly, the detection of aliphatic hydrocarbons in the diffuse interstellar medium, IDPs, and meteorites and not in dense molecular clouds poses an evolutionary problem. The presence of the aliphatic groups in the diffuse dust, in comets, IDPs, and meteorites may be deceptive and may not necessarily imply a direct evolutionary connection between the organics in the diffuse ISM (aliphatic component observed, CH_2/CH_3 ratio of 2.2), the organics in dense clouds where planetary systems formed (aliphatic component not observed) and organics in comets, IDPs, and meteorites (aliphatic component observed, but with a CH_2/CH_3 ratio higher than 5). However, although this evolutionary link is not established, various scenarios might be tested on the grounds of laboratory experiments where the input material may be synthetic amorphous carbon and its evolution might be followed by infrared spectroscopy within a reaction chamber in which the conditions prevailing in the primitive solar nebula may be somewhat reproduced.

CONCLUSIONS

Raman data, Infrared spectra, and associated FESEM/EDX were acquired from 16 particles collected from comet 81P/Wild 2 by the Stardust spacecraft. These data indicate that cometary grains are rich in various and complex organic compounds and show compositional and structural heterogeneities. These heterogeneities are detected even among particles coming from the same impact track, suggesting the original particle consisted of a mixture of different subgrains of various sizes and compositions, in accordance with the results obtained on most Wild 2 samples (Brownlee et al. 2006; Flynn et al. 2006; Hörz et al. 2006; McKeegan et al. 2006; Sandford et al. 2006; Zolensky et al. 2006).

While there is some evidence of the possible processing of the organics by the impact processes, the presence of a) heterogeneity, b) Raman band parameters consistent with highly "primitive" materials, and c) some materials with low degrees of oxidation, all suggest that some of the material survived collection relatively unscathed.

The Raman D and G bands indicate aromatic hydrocarbons are present, and occasionally aliphatics are seen. The IR data indicate that aliphatic materials are present and occasionally show features consistent with the presence of aromatics.

The D and G band parameters of the Stardust samples scatter across the entire meteoritic field and are best matched to IDPs. Micro-IR data are also most similar to those of IDPs. The CH_2/CH_3 ratios measured from the Stardust particles are higher than those observed for the diffuse ISM, but are similar to the ratios seen in IDPs.

Micro-IR spectroscopy suggests hydrated minerals may be present in two of the particles, one of which may also contain carbonates. The rarity of these mineral phases within Stardust samples in general suggests further investigations of these two particles using other analytical techniques would be extremely useful.

Acknowledgments–The work done by the LANDS team (Italy) was supported by the Università di Napoli "Parthenope," the Istituto Nazionale di Astrofisica and the MIUR program

PRIN/2005. The LANDS team thanks Assing s.p.a. personnel for technical assistance. The work at Institut d'Astrophysique Spatiale (Orsay, France) was supported by the French Space Agency CNES. The French team also wants to thank Giles Montagnac of ENS-Lyon for the help in handling the Raman analyses, Hugues Leroux of LSPES, Lille for his collaboration in the SEM-FEG/EDX analyses and Emmanuel Dartois for providing us the GC-SGRA data. SS is grateful for support from the Stardust Mission Project. The CIW team thanks NASA for its support of this work through the Sample Return Laboratory Instrument and Data Analysis and Stardust Participating Scientist programs. BW thanks the McDonnell Center for the Space Sciences at Washington University in St. Louis for support. We are grateful to the dedicated work of the Stardust Sample Curation Team. We acknowledge the review work done by the anonymous reviewer and by Mark Sephton.

Editorial Handling—Dr. Ian Lyon

REFERENCES

Alexander C. M. O'D., Russell S. S., Arden J. W., Ash R. D., Grady M. M., and Pillinger C. T. 1998. The origin of chondritic macromolecular organic matter: A carbon and nitrogen isotope study. *Meteoritics & Planetary Science* 33:603–622.

Alexander C. M. O'D., Fogel M., Yabuta H., and Cody G. D. 2007. The origin and evolution of chondrites recorded in the elemental and isotopic compositions of their macromolecular organic matter. *Geochimica et Cosmochimica Acta* 71:4380–4403.

Allamandola L. J., Sandford S. A., Tielens A. G. G. M., and Herbst T. M. 1992. Infrared spectroscopy of dense clouds in the C-H stretch region—Methanol and "diamonds." *The Astrophysical Journal* 399:134–146.

Anders E. 1989. Prebiotic organic matter from comets and asteroids. *Nature* 342:255–257.

Bajt S., Flynn G., Matrajt G., Sandford S., Snead C., and Westphal A. Forthcoming. Infrared spectroscopy of Wild 2 particle hypervelocity tracks in Stardust aerogel: Evidence for the presence of volatile organics in comet dust. *Meteoritics & Planetary Science*.

Baratta G. A., Arena M. M., Strazzulla G., Colangeli L., Mennella V., Palumbo P., and Bussoletti E. 1996. Raman spectroscopy of ion irradiated amorphous carbons. *Nuclear Instruments and Methods in Physics Research B* 116:195–199.

Baratta G. A. Mennella V., Brucato J. R., Colangeli L., Leto G., Palumbo M. E., and Strazzulla G. 2004. Raman spectroscopy of ion-irradiated interplanetary carbon dust analogues. *Journal of Raman Spectroscopy* 35:487–496.

Bernstein M. P., Sandford S. A., Allamandola L. J., and Chang S. 1994. Infrared spectrum of matrix-isolated hexamethylenetetramine in Ar and H_2O at cryogenic temperatures. *Journal of Physical Chemistry* 98:12206–12210.

Bernstein M. P., Sandford S. A., Allamandola L. J., Chang S., and Scharberg M. A. 1995. Organic compounds produced by photolysis of realistic interstellar and cometary ice analogs containing methanol. *The Astrophysical Journal* 454:327–344.

Bernstein M. P., Sandford S. A., and Allamandola L. J. 1997. The infrared spectra of nitriles and related compounds frozen in Ar and H_2O. *The Astrophysical Journal* 476:932–942.

Bernstein M. P., Sandford S. A., Allamandola L. J., Gillette J. S., Clemett S. J., and Zare R. N. 1999. UV irradiation of polycyclic aromatic hydrocarbons in ices: Production of alcohols, quinones, and ethers. *Science* 283:135–1138.

Bernstein M. P., Dworkin J. P., Sandford S. A., Cooper G. W., and Allamandola L. J. 2002. The formation of racemic amino acids by ultraviolet photolysis of interstellar ice analogs. *Nature* 416: 401–403.

Beyssac O., Goffé B., Petitet J.-P., Froigneux E., Moreau M., and Rouzaud J.-N. 2003. On the characterization of disordered and heterogeneous carbonaceous materials by Raman spectroscopy. *Spectrochimica Acta Part A* 59:2267–2276.

Bohren C. F. and Huffman D. R. 1983. *Absorption and scattering of light by small particles*. New York: Wiley Interscience.

Bockelée-Morvan D., Crovisier J., Mumma M., and Weaver H. 2004. The volatiles composition of comets. In *Comets II*, edited by Festou M., Keller H. U., and Weaver H. A. Tucson, Arizona: The University of Arizona Press. pp. 391–423.

Bonal L., Quirico E., Bourot-Denise M., and Montagnac G. 2006. Determination of the petrologic type of CV3 chondrites by Raman spectroscopy of included organic matter. *Geochimica et Cosmochimica Acta* 70:1849–1863.

Borg J., Djouadi Z., Grossemy F., Eichert D., Martinez-Criado G., Westphal A. J., Deboffle D., Snead C. J., and Somogyi A. 2006. Synchrotron X-rays in-situ analyses of extraterrestrial grains trapped in aerogel. *Advance in Space Research* 38:2068–2074.

Bradley J. P. 2003. Interplanetary dust particles. In *Meteorites, comets, and planets*, edited by Davies A. M. Treatise on Geochemistry, vol. 1. Amsterdam: Elsevier. pp. 689–711.

Brooke T. Y., Sellgren K., and Geballe T. R. 1999. New 3 micron spectra of Young Stellar Objects with H_2O ice bands. *The Astrophysical Journal* 517:883–900.

Brooke T. Y., Sellgren K., and Smith R. G. 1996. A study of absorption features in the 3 micron spectra of molecular cloud sources with H_2O ice bands. *The Astrophysical Journal* 459:209–215.

Brownlee D. E., Joswiak D. J., Schlutter D. J., Pepin R. O., Bradley J. P., and Love S. G. 1995. Identification of individual cometary IDPs by thermally stepped He release (abstract). 26th Lunar and Planetary Science Conference. pp.183–184.

Brownlee D. E. 2003. Comets. In *Meteorites, comets, and planets*, edited by Davies A. M. Treatise on Geochemistry, vol. 1. Amsterdam: Elsevier. pp. 663–688.

Brownlee D., Tsou P., Aléon J., Alexander C. M. O'D., Araki T., Bajt S., Baratta G. A., Bastien R., Bland P., Bleuet P., Borg J., Bradley J. P., Brearley A., Brenker F., Brennan S., Bridges J. C., Browning N., Brucato J. R., Brucato H., Bullock E., Burchell M. J., Busemann H., Butterworth A., Chaussidon M., Cheuvront A., Chi M., Cintala M. J., Clark B. C., Clemett S. J., Cody G., Colangeli L., Cooper G., Cordier P., Daghlian C., Dai Z., D'Hendecourt L., Djouadi Z., Dominguez G., Duxbury T., Dworkin J. P., Ebel D., Economou T. E., Fairey S. A. J., Fallon S., Ferrini G., Ferroir T., Fleckenstein H., Floss C., Flynn G., Franchi I. A., Fries M., Gainsforth Z., Gallien J.-P., Genge M., Gilles M. K., Gillet P., Gilmour J., Glavin D. P., Gounelle M., Grady M. M., Graham G. A., Grant P. G., Green S. F., Grossemy F., Grossman L., Grossman J., Guan Y., Hagiya K., Harvey R., Heck P., Herzog G. F., Hoppe P., Hörz F., Huth J., Hutcheon I. D., Ishii H., Ito M., Jacob D., Jacobsen C., Jacobsen S., Joswiak D., Kearsley A. T., Keller L., Khodja H., Kilcoyne A. L. D., Kissel J., Krot A., Langenhorst F., Lanzirotti A., Le L., Leshin L., Leitner J., Lemelle L., Leroux H., Liu M.-C., Luening K., Lyon I., MacPherson G., Marcus M. A., Marhas K., Matrajt G., Meibom A., Mennella V., Messenger K., Mikouchi T., Mostefaoui S., Nakamura T., Nakano T., Newville M., Nittler L. R., Ohnishi I., Ohsumi K., Okudaira K., Papanastassiou D. A.,

Palma R., Palumbo M. E., Pepin R. O., Perkins D., Perronnet M., Pianetta P., Rao W., Rietmeijer F., Robert F., Rost D., Rotundi A., Ryan R., Sandford S. A., Schwandt C. S., See T. H., Schlutter D., Sheffield-Parker J., Simionovici A., Simon S., Sitnitsky I., Snead C. J., Spencer M. K., Stadermann F. J., Steele A., Stephan T., Stroud R., Susini J., Sutton S. R., Taheri M., Taylor S., Teslich N., Tomeoka K., Tomioka N., Toppani A., Trigo-Rodríguez J. M., Troadec D., Tsuchiyama, A. Tuzolino A. J., Tyliszczak T., Uesugi K., Velbel M., Vellenga J., Vicenzi E., Vincze L., Warren J., Weber I., Weisberg M., Westphal A. J., Wirick S., Wooden D., Wopenka B., Wozniakiewicz P., Wright I., Yabuta H., Yano H., Young E. D., Zare R. N., Zega T., Ziegler K., Zimmerman L., Zinner E., and Zolensky M. E. 2006. Comet 81P/Wild 2 under a microscope. *Science* 314:1711–1716.

Brucato J. R., Baratta G. A., and Strazzulla G. 2006a. An IR study of pure and ion irradiated frozen formamide. *Astronomy and Astrophysics* 455:395–399.

Brucato J. R., Strazzulla G., Baratta G. A., Rotundi A., and Colangeli L. 2006b. Cryogenic synthesis of molecules of astrobiological interest: Catalytic role of cosmic dust analogues. *Origin of Life and Evolution of Biosphere* 36:451–457.

Busemann H., Alexander C. M. O'D. and Nittler L. R. 2007. Characterization of insoluble organic matter in primitive meteorites by micro-Raman spectroscopy. *Meteoritics & Planetary Science* 42:1387–1416.

Cannia R., Strazzulla G., Compagnini G., and Baratta G. A. 1994. Vibrational spectroscopy of ion-irradiated pentacene. *Infrared Physics & Technology* 6:791–800.

Cataldo F., Baratta G. A., Ferrini G., and Strazzulla G. 2003. He^+ ion bombardment of C70 fullerene: An FT-IR and Raman study. *Fullerenes Nanotubes and Carbon Nanostructures* 11:191–199.

Chiar J. E., Adamson A. J., and Whittet D. C. B. 1996. Three micron hydrocarbon and methanol absorption in Taurus. *The Astrophysical Journal* 472:665–672.

Chiar J. E., Tielens A. G. G. M., Whittet D. C. B., Schutte W. A., Boogert A. C. A., Lutz D., van Dishoeck E. F., and Bernstein M. P. 2000. The composition and distribution of dust along the line of sight toward the Galactic Center. *The Astrophysical Journal* 537:749–762.

Chizmadia L. J. 2007. Reproduction of phyllosilicate textures in CM2 chondrites during experimental hydration of amorphous silicate smokes (abstract #1005). 38th Lunar and Planetary Science Conference. CD-ROM.

Chyba C. F. and Sagan C. 1997. Comets as a source of prebiotic organic molecules for the early Earth. In *Comets and the origin and evolution of life*, edited by Thomas P. J., Chyba C. F., and McKay C. P. New York: Springer-Verlag. pp. 147–174.

Cody G. Ade H., Alexander C. M. O'D, Araki T., Butterworth A., Fleckenstein H., Flynn G., Gilles M. K., Jacobsen C., Kilcoyne A. L. D., Messenger K., Sandford S. A., Tyliszczak T., Westphal A. J., Wirick S., and Yabuta H. 2008. Quantitative organic and light-element analysis of comet 81P/Wild 2 particles using C-, N-, and O-μ-XANES. *Meteoritics & Planetary Science* 43. This issue.

Compagnini G. and Baratta G. A. 1992. Polarized Raman spectroscopy in ion irradiated graphite. *Applied Physics Letters* 61:1796–1798.

Court R. W., Sephton M. A., Parnell J., and Gilmour I. 2006. The alteration of organic matter in response to ionising irradiation: Chemical trends and implications for extraterrestrial sample analysis. *Geochimica et Cosmochimica Acta* 70:1020–1039.

Court R. W., Sephton M. A., Parnell J., and Gilmour I. 2007. Raman spectroscopy of irradiated organic matter. *Geochimica et Cosmochimica Acta* 71:2547–2568.

Crovisier J. 2004. The molecular complexity of comets. In *Astrobiology: Future perspectives*, edited by Ehrenfreud P., Irvine W., Owen T., Becker L., Blank J., Brucato J. R., Colangeli L., Derenne S., Dutrey A., Despois D., and Lazcano A. Dordrecht: Kluwer. pp. 179–199.

Dartois E., Marco O., Muñoz-Caro G. M., Brooks K., Deboffle D., and D'Hendecourt L. 2004a. Organic matter in Seyfert 2 nuclei: Comparison with our Galactic center lines of sight. *Astronomy and Astrophysics* 423:549–558.

Dartois E., Munoz-Caro G. M., Deboffle D., and D'Hendecourt L. 2004b. Diffuse interstellar medium organic polymers. Photoproduction of the 3.4, 6.85 and 7.25 micron features, *Astronomy and Astrophysics Letters* 423:L33–36.

Dartois E., Muñoz-Caro G. M., Deboffle D., Montagnac G., and D'Hendecourt L. 2005. Ultraviolet photoproduction of ISM dust. Laboratory characterization and astrophysical relevance. *Astronomy and Astrophysics* 432:895–908.

Djouadi Z., Matrajt G., Raynal P. I., Borg J., and D'Hendecourt L. 2003. FTIR and Raman analyses of the carbon in Tagish Lake meteorite (abstract #5075). *Meteoritics & Planetary Science* 38.

D'Hendecourt L. and Allamandola L. J. 1986. Time dependent chemistry in dense molecular clouds. III. Infrared band cross sections of molecules in the solid state at 10K. *Astronomy and Astrophysics Supplement Series* 64:453–467.

Durand B., ed. 1980. *Kerogen: Insoluble organic matter from sedimentary rocks*. Editions TECHNIP. 550 p.

Dworkin J. P., Deamer D. W., Sandford S. A., and Allamandola L. J. 2001. Self-assembling amphiphilic molecules: Synthesis in simulated interstellar/precometary ices. *Proceedings of the National Academy of Sciences* 98:815–819.

Elman B. S., Dresselhaus M. S., Dresselhaus G., Maby E. W., and Mazurek H. 1981. Raman scattering from ion-implanted graphite. *Physical Review B* 24:1027–1034.

Everall N. J. and Lumsdon J. 1991. The effect of laser-induced heating upon the vibrational Raman spectra of graphites and carbon fibres. *Carbon* 29:133–137.

Ferini G., Baratta G. A., and Palumbo M. E. 2004. A Raman study of ion-irradiated icy mixtures. *Astronomy and Astrophysics* 414:757–766.

Ferrari A. C. and Robertson J. 2000. Interpretation of Raman spectra of disordered and amorphous carbon. *Physical Review B* 61: 14,095–14,107.

Ferrari A. C. and Robertson J. 2001. Resonant Raman spectroscopy of disordered, amorphous, and diamondlike carbon. *Physical Review B* 64:id.075414.

Ferrini G., Colangeli L., Mennella V., Palomba E., Palumbo P., Rotundi A., Westphal A. J., and Borg J. 2001. COMET-99 OAC Aerogel samples: preliminary FESEM-EDX analyses, *Proceedings of the CNES Symposium "International Scientific Cooperation onboard MIR,"* Lyon, France, 19–21 March 2001. p. 373.

Flynn G., Bleuet P., Borg J., Bradley J. P., Brenker F. E., Brennan S., Bridges J., Brownlee D. E., Bullock E. S., Burghammer M., Clark B. C., Dai Z. R., Daghlian C. P., Djouadi Z., Fakra S., Ferroir T., Floss C., Franchi I. A., Gainsforth Z., Gallien J. P., Gillet P., Grant P. G., Graham G. A., Green S. F., Grossemy F., Heck P. R., Herzog G. F., Hoppe P., Hörz F., Huth J., Ignatyev K., Ishii H. A., Janssens K., Joswiak D., Kearsley A. T., Khodja H., Lanzirotti A., Leitner J., Lemelle L., Leroux H., Luening K., MacPherson G. J., Marhas K. K., Marcus M. A., Matrajt G., Nakamura T., Nakamura-Messenger K., Nakano T., Newville M., Papanastassiou D. A., Pianetta P., Rao W., Riekel C., Rietmeijer F. J. M., Rost D., Schwandt C. S., See T. H., Sheffield-Parker J., Simionovici A., Sitnisky I., Snead C. J., Stadermann F. J., Stephan T., Stroud R. M., Susini J., Susuki Y., Sutton S. R., Taylor S., Teslich N., Troadec D., Tsou P.,

Tsuchiyama A., Uesigi K., Vekemans B., Vicenzi E. P., Vincze L., Westphal A. J., Wosniakiewicz P., Zinner E., and Zolensky M. E. 2006. Elemental compositions of comet 81P/Wild 2 samples collected by Stardust. *Science* 314:1731–1735.

Flynn G. J., Keller L. P., Feser M., Wirick S., and Jacobsen C. 2003. The origin of organic matter in the solar system: Evidence from the interplanetary dust particles. *Geochimica et Cosmochimica Acta* 67:4791–4806.

Fomenkova M. N. 1999. On the organic refractory component of cometary dust. *Space Science Reviews* 90:109–114.

Foster N. J., Burchell M. J., Creighton J. A., and Kearsley A. T. 2007. Does capture in aerogel change carbonaceous Raman D and G bands? (abstract #1647). 38th Lunar and Planetary Science Conference. CD-ROM.

Gil-Hutton R. 2002. Color diversity among Kuiper belt objects: The collisional resurfacing model revisited. *Planetary and Space Science* 50:57–62.

Grewing M., Praderie F., and Reinhard R., eds. 1987. *Exploration of Halley's comet*. Berlin Heidelberg, New York, London, Paris, Tokyo: Springer.

Grossemy F., Borg J., and Simionovici A. 2006. In-situ Fe-XANES study of grains trapped in aerogel: an analytical test for the interpretation of Stardust samples analyses. *Meteoritics & Planetary Science* 41:5276.

Hill H. G. M. and Nuth J. A. 2003. The catalytic potential of cosmic dust: Implications for prebiotic chemistry in the solar nebula and other protoplanetary systems. *Astrobiology* 3:291–304.

Hollis J. M., Jewell P. R., Lovas F. J., Remijan A., and Møllendal H. 2004. green bank telescope detection of new interstellar aldehydes: Propenal and propanal. *The Astrophysical Journal* 610:L21–L24.

Hörz F., Bastien R., Borg J., Bradley J. P., Bridges J. C., Brownlee D. E., Burchell M. J., Chi M., Cintala M. J., Dai Z. R., Djouadi Z., Dominguez D., Economou T. E., Fairey S. A. J., Floss C., Franchi I. A., Graham G. A., Green S. F., Heck P., Hoppe P., Huth J., Ishii H., Kearsley A. T., Kissel J., Leitner J., Leroux H., Marhas K., Messenger K., Schwandt C. S., See T. H., Snead C., Stadermann F. J., Stephan I. T., Stroud R., Teslich N., Trigo-Rodríguez J. M., Tuzzolino A. J., Troadec D., Tsou P., Warren J., Westphal A., Wozniakiewicz P., Wright I., and Zinner E. 2006. Impact features on Stardust: Implications for comet 81P/Wild 2 dust. *Science* 314:1716–1719.

Hudgins D. M. and Sandford S. A. 1998a. Infrared spectroscopy of matrix-isolated polycyclic aromatic hydrocarbons 1. PAHs containing 2 to 4 rings. *Journal of Physical Chemistry* 102: 329–343.

Hudgins D. M. and Sandford S. A. 1998b. Infrared spectroscopy of matrix-isolated polycyclic aromatic hydrocarbons 2. PAHs containing 5 or more rings. *Journal of Physical Chemistry* 102: 344–352.

Hudgins D. M. and Sandford S. A. 1998c. Infrared spectroscopy of matrix-isolated polycyclic aromatic hydrocarbons 3. fluoranthene and the benzofluoranthenes. *Journal of Physical Chemistry B*: 353–360.

Irvine W. M., Schloerb F. P., Crovisier J., Fegley B., Jr., and Mumma M. J. 2000. Comets: A link between interstellar and nebular chemistry. In *Protostars and planets IV*, edited by Mannings V., Boss A., and Russell S. Tucson: The University of Arizona Press. pp. 1159–1200.

Joswiak D. J., Matrajt G., Brownlee D. E., Westphal A. J., and Snead C. J. 2007. A roedderite-bearing terminal particle from Stardust Track 56: Comparison with rare peralkaline chondrules in ordinary chondrites (abstract #1338). 38th Lunar and Planetary Science Conference. CD-ROM.

Keller and Messenger 2005. The nature and origin of interplanetary dust: High-temperature components. In *Chondrites and the protoplanetary disk*, edited by Krot A. N., Scott E. R. D., and Reipurth B. ASP Conference Series, vol. 341. pp. 657–667.

Keller L. P., Messenger S., Flynn G. J., Clemett S., Wirick S., and Jacobsen C. 2004. The nature of molecular cloud material in interplanetary dust. *Geochimica et Cosmochimica Acta* 68: 2577–2589.

Keller L. P., Bajt S., Baratta G. A., Borg J., Bradley J. P., Brownlee D. E., Brucato J. R., Burchell M. J., Busemann H., Colangeli L., D'Hendecourt L., Djouadi Z., Ferrini G., Flynn G., Franchi I. A., Fries M., Grady M.M., Gilles M. K., Graham A., Grossemy F., Kearsley A., Matrajt G., Nakamura-Messanger K., Mennella V., NittlerL. R., Palumbo M. E., Rotundi A., Sandford S.A., Snead C. J., Stadermann F. J., Steele A., Tsou P., Wooden D., and Zolensky M. 2006. Organics captured from comet 81P/Wild 2 by the Stardust spacecraft. *Science* 314:1728–1731.

Kissel J. and Krueger F. R. 1987. The organic component in dust from comet Halley as measured by the PUMA mass spectrometer on board Vega 1. *Nature* 326:755–760.

Kuan Y., Charnley S. B., Huang H., Tseng W., and Kisiel Z. 2003. Interstellar glycine. *The Astrophysical Journal* 593:848–867.

Langhoff S. R., Bauschlicher Jr. C. W., Hudgins D. M., Sandford S. A., and Allamandola L. J. 1998. Infrared spectra of substituted polycyclic aromatic hydrocarbons. *Journal of Physical Chemistry A* 102:1632–1646.

Leroux H., Rietmeijer F. J. M., Velbel M. A., Brearley A. J., Jacob D., Langenhorst F., Bridges J. C., Zega T. J., Stroud R. M., Cordier P., Harvey R. P., Lee M., Gounelle M., and Zolensky M. E. 2008. A TEM study of thermally modified comet 81P/Wild 2 dust particles by interactions with the aerogel matrix during the Stardust capture process. *Meteoritics & Planetary Science* 43. This issue.

Lisse C. M., Van Cleve J., Adams A. C., A'Hearn M. F., Fernández Y. R., Farnham T. L., Armus L., Grillmair C. J., Ingalls J., Belton M. J. S., Groussin O., McFadden L. A., Meech K. J., Schultz P. H., Clark B. C., Feaga L. M., Sunshine J. M. 2006. Spitzer spectral observations of the deep impact ejecta. *Science* 313:635.

Matrajt G., Borg J., Raynal P. I., Djouadi Z., D'Hendecourt L., Flynn G., and Deboffle D. 2004. FTIR and Raman analyses of the Tagish Lake meteorite: Relationship with the aliphatic hydrocarbons observed in the diffuse interstellar medium. *Astronomy and Astrophysics* 416:983–990.

Matrajt G., Muñoz-Caro G. M., Dartois E., D'Hendecourt L., Deboffle D., and Borg J. 2005. FTIR analysis of the organics in IDPs: comparison with the IR spectra of the diffuse interstellar medium. *Astronomy and Astrophysics* 433:979–995.

Matthews M. J., Pimenta M. A., Dresselhaus G., Dresselhaus M. S., and Endo M. 1999. Origin of dispersive effects of the Raman D band in carbon materials. *Physical Review B* 59: R6585–R6588.

McKeegan K. D., Aléon J., Bradley J., Brownlee D., Busemann H., Butterworth A., Chaussidon M., Fallon S., Floss C., Gilmour J., Gounelle M., Graham G., Guan Y., Heck P. R., Hoppe P., Hutcheon I. D., Huth J., Ishii H., Ito M., Jacobsen S. B., Kearsley A., Leshin L. A., Liu M.-C., Lyon I., Marhas K., Marty B., Matrajt G., Meibom A., Messenger S., Mostefaoui S., Mukhopadhyay S., Nakamura-Messenger K., Nittler L., Palma R., Pepin R. O., Papanastassiou D. A., Robert F., Schlutter D., Snead C. J., Stadermann F. J., Stroud R., Tsou P., Westphal A., Young E. D., Ziegler K., Zimmermann L., and Zinner E. 2006. Isotopic compositions of cometary matter returned by Stardust. *Science* 314:1724–1727.

Mennella V. 2006. Activation energy of CH bond formation in carbon grains irradiated with hydrogen atoms. *The Astrophysical Journal* 647:L49–L52.

Mennella V., Baratta G. A., Esposito A., Ferrini G., and Pendleton Y. J. 2003. The effects of ion irradiation on the evolution of the carrier of the 3.4 micron interstellar absorption band. *The Astrophysical Journal* 587:727–738.

Mennella V., Brucato J. R., Colangeli L., and Palumbo P. 2002. CH bond formation in carbon grains by exposure to atomic hydrogen: The evolution of the carrier of the interstellar 3.4 micron band. *The Astrophysical Journal* 569:531–540.

Mikouchi T., Tachikawa O., Hagiya K., Ohsumi K., Suzuki Y., Uesugi K., Takeuchi A., and Zolensky M. E. 2007. Mineralogy and crystallography of comet 81P/Wild 2 particles (abstract #1946). 38th Lunar and Planetary Science Conference. CD-ROM.

Muñoz-Caro G. M., Ruiterkamp R., Schutte W. A., Greenberg J. M., and Mennella V. 2001. UV photodestruction of CH bonds and the evolution of the 3.4 mm feature carrier. I. The case of aliphatic and aromatic molecular species. *Astronomy and Astrophysics* 367: 347–354.

Muñoz-Caro G. M., Matrajt G., Dartois E., Nuevo M., D'Hendecourt L., Deboffle D., Montagnac G., Chauvin N., Boukari C., and Le Du D. 2006. Nature and evolution of the dominant carbonaceous matter in interplanetary dust particles: Effects of irradiation and identification with a type of amorphous carbon. *Astronomy and Astrophysics* 459:147–159.

Musumeci P., Calcagno L., Makhtari A., Baeri P., Compagnini G., and Pirri C. F. 2000. *Nuclear Instruments and Methods in Physics Research B* 166:404–409.

Negri F., di Donato E., Tommasini M., Castiglioni C., and Zerbi G. 2004. Resonance Raman contribution to the D band of carbon materials: Modeling defects with quantum chemistry. *Journal of Chemical Physics* 120:11889–11900.

Nelson R. M., Rayman M. D., and Weaver H. A. 2004. The Deep Space 1 encounter with comet 19P/Borrelly. *Icarus* 167:1–3.

Neuhaeuser M., Hilgers H., Joeris P., White R., and Windeln J. 2000. Raman spectroscopy measurements of DC-magnetron sputtered carbon nitride_a-C:N/thin films for magnetic disk coatings. *Diamond and Related Materials* 9:1500–1505.

Oró J., Lazcano A., and Ehrenfreud P. 2006. Comets and the origin and evolution of life. In *Comets and the origin and evolution of life*, edited by Thomas P. J., Hicks R. D., Chyba C. F., and McKay C. P. Berlin-Heidelberg: Springer. pp. 1–28.

Palumbo M. E., Ferrini G., and Baratta G. A. 2004. Infrared and Raman spectroscopies of refractory residues left over after ion irradiation of nitrogen-bearing icy mixtures. *Advances in Space Research* 33:49–56.

Pasteris J. D. and Wopenka B. 1991. Raman spectra of graphite as indicators of degree of metamorphism. *Canadian Mineralogist* 29:1–9.

Pasteris J. D. and Wopenka B. 2004. Necessary, but not sufficient: Raman identification of disordered carbon as a signature of ancient life. *Astrobiology* 3:727–738.

Pendleton Y. J., Sandford S. A., Allamandola L. J., Tielens A. G. G. M., and Sellgren K. 1994. Near-infrared absorption spectroscopy of interstellar hydrocarbon grains. *The Astrophysical Journal* 437:683–696.

Pendleton Y. J. and Allamandola L. J. 2002. The organic refractory material in the diffuse interstellar medium: Mid-infrared spectroscopic constraints. *The Astrophysical Jjournal (Suppl. Ser.)* 138:75–98.

Quirico E., Raynal P.-I., and Buorot-Denise M. 2003. Metamorphic grade of organic matter in six unequilibrated ordinary chondrites. *Meteoritics & Planetary Science* 38:795–811.

Quirico E., Raynal P.-I., Borg J., and D'Hendecourt L. 2005. A micro-Raman survey of 10 IDPs and 6 carbonaceous chondrites. *Planetary and Space Science* 53:1443–1448.

Raynal P.-I. 2003. Étude en laboratoire de matière extraterrestre: implications pour la physico-chimie du Système Solaire primitif. Ph.D. Thesis. Université de Paris 6, Paris.

Raynal P. I., Quirico E., Borg J., Deboffle D., Dumas P., D'Hendecourt L., Bibring J.-P., and Langevin Y. 2000. Synchrotron infrared microscopy of micron-sized extraterrestrial grains. *Planetary and Space Science* 48:1329–1339.

Raynal P. I., Quirico E., Borg J., and D'Hendecourt L. 2001. Micro-Raman survey of the carbonaceous matter structure in stratospheric IDPs and carbonaceous chondrites (abstract #1341). 32nd Lunar and Planetary Science Conference. CD-ROM.

Rietmeijer F. J. M. 2002. The earliest chemical dust evolution in the solar nebula. *Chemie der Erde* 62:1–45.

Rietmeijer F. J. M., Rotundi A., and Heymann D. 2004. C60 and giant fullerenes in soot condensed in vapors with variable C/H_2 ratio. *Fullerenes, Nanotubes and Carbon Nanostructures* 12:659–680.

Rodgers S. D. and Charnley S. B. 2004. Physical processes and chemical reactions in cometary comae. In *Comets II*, edited by Festou M., Keller H. U., and Weaver H. A., Tucson, Arizona: The University of Arizona Press. pp. 505–522.

Rotundi A., Rietmeijer F. J. M., Colangeli L., Mennella V., Palumbo P., and Bussoletti E. 1998. Identification of carbon forms in soot materials of astrophysical interest. *Astronomy and Astrophysics* 329:1087–1096.

Rotundi A., Ferrini G., Baratta G. A., Palumbo M. E., Palomba E., and Colangeli L. 2007. Combined micro-infrared and micro-Raman measurements on stratospheric interplanetary dust particles. In *Dust in planetary systems*, edited by Krüger H. and Graps A. ESA Publication SP-643. pp. 149–153.

Saladino R., Crestini C., Ciciriello F., Costanzo G., Negri R., and Di Mauro E. 2004. A novel synthesis of biomolecular precursor. In *Astrobiology: Future perspectives*, edited by Ehrenfreud P., Irvine W., Owen T., Becker L., Blank J., Brucato J. R., Colangeli L., Derenne S., Dutrey A., Despois D., and Lazcano A. Dordrecht: Kluwer. pp. 393–413.

Saladino R., Crestini C., Neri V., Brucato J. R., Colangeli L., Ciciriello F., Di Mauro E., and Costanzo G. 2005. Synthesis-degradation of nucleic acids components by formamide and cosmic dust analogues. *ChemBioChem* 6:1368–1374.

Salisbury J. W., Walter L. S., Vergo N., and D'Aria D. M. 1991. *Infrared (2.1–25 μm) spectra of minerals*. John Hopkins University Press.

Sandford S. A., Allamandola, L. J., Tielens A. G. G. M., Sellgren K., Tapia M., and Pendleton Y. 1991. The interstellar C-H stretching band near 3.4 microns–Constraints on the composition of organic material in the diffuse interstellar medium. *The Astrophysical Journal* 371:607–620.

Sandford S. A., Aléon J., Alexander C. M. O'D., Araki T., Bajt S., Baratta G. A., Borg J., Bradley J. P., Brownlee D. E., Brucato J. R., Burchell M. J., Busemann H., Butterworth A., Clemett S. J., Cody G., Colangeli L., Cooper G., D'Hendecourt L., Djouadi Z., Dworkin J. P., Ferrini G., Fleckenstein H., Flynn G. J., Franchi I. A., Fries M., Gilles M. K., Glavin D. P., Gounelle M., Grossemy F., Jacobsen C., Keller L. P., Kilcoyne A. L. D., Leitner J., Matrajt G., Meiborn A., Mennelle V., Mostefaoui S., Nittler L.R., Palumbo M. E., Papanastassiou D. A., Robert F., Rotundi A., Snead C. J., Spencer M. K., Stadermann F. J., Steele A., Stephan T., Tsou P., Tyliszczak T., Westphal A. J., Wirick S., Wopenka B., Yabuta H., Zare R. N., and Zolensky M. E. 2006. Organics captured from comet 81P/Wild 2 by the Stardust spacecraft. *Science* 314:1720–1724.

Schopf J. W., Kudryavtsev A. B., Agresti D. G., Czaja A. D., and Wdowiak T. J. 2005. Raman imagery: A new approach to assess the geochemical maturity and biogenicity of permineralized precambrian fossils. *Astrobiology* 5:333–371.

Sephton M. A., Pillinger C. T., and Gilmour I. 2001. Normal alkanes in meteorites: Molecular $\delta^{13}C$ values indicate an origin by terrestrial contamination. *Precambrian Research* 106:45–56.

Sephton M. A. 2002. Organic compounds in carbonaceous meteorites. *Natural Product Reports* 19:292–311.

Stadermann F. J., Floss C., and Wopenka B. 2006. Circumstellar aluminum oxide and silicon carbide in interplanetary dust particles. *Geochimica et Cosmochimica Acta* 70:6168–6179.

Strazzulla G. and Baratta G. A. 1992. Carbonaceous material by ion irradiation in space. *Astronomy and Astrophysics* 266:434–438.

Strazzulla G. and Johnson R. E. 1991. Irradiation effects on comets and cometary debries. In *Comets in the post-Halley era*, edited by R. Newburn Jr., M. Neugebauer, and J. Rahe. Dordrecht: Kluwer Academic. pp. 243–275.

Strazzulla G., Baratta G. A., and Spinella F. 1995. Production and evolution of carbonaceous material by ion irradiation in space. *Advances in Space Research* 15:385–399.

Strazzulla G., Baratta G. A., Johnson R. E., and Donn B. 1991. Primordial comet mantle: Irradiation production of a stable, organic crust. *Icarus* 91:101–104.

Strazzulla G., Baratta G. A., and Palumbo M. E. 2001. Vibrational spectroscopy of ion-irradiated ices. *Spectrochimica Acta* 57:825–842.

Strazzulla G., Cooper J. F., Christian E. R., and Johnson R. E. 2003. Ion irradiation of TNOs: From the fluxes measured in space to the laboratory experiments. *Comptes Rendus Physique* 4:791–801.

Szczepanski J. and Vala, M. 1993. Infrared frequencies and intensities for astrophysically important polycyclic aromatic hydrocarbon cations. *The Astrophysical Journal* 414:646–655.

Tuinstra F. and Koenig J. 1970. Raman spectrum of graphite. *Journal of Chemical Physics* 53:1126–1130.

Westphal A. J., Snead C., Butterworth A., Graham G. A., Bradley J. P., Bajt S., Grant P. G., Bench G., Brennan S., and Pianetta P. 2004. Aerogel keystones: Extraction of complete hypervelocity impact events from aerogel collectors. *Meteoritics & Planetary Science* 39:1375–1386.

Whittet D. C. B., Boogert A. C. A., Gerakines P. A., Schutte W., Tielens A. G. G. M., de Graauw T., Prusti T., van Dishoeck E. F., Wesselius P. R., and Wright C. M. 1997. Infrared spectroscopy of dust in the diffuse interstellar medium toward Cygnus OB2 No. 12. *The Astrophysical Journal* 490:729–734.

Wirick S., Leroux H., Tomeoka K., Zolensky M., Flynn G. J., Tyliszczak T., Butterworth A., Tomioka N., Ohnishi I., Nakamura-Messenger K., Sandford S., Keller L., and Jacobsen C. 2007. Carbonates found in Stardust aerogel tracks (abstract #1946). 38th Lunar and Planetary Science Conference. CD-ROM.

Wopenka B. 1988. Raman observations on individual interplanetary dust particles. *Earth and Planetary Science Letters* 88:221–231.

Zolensky M. E., Zega T. J., Yano H., Wirick S., Westphal A. J., Welsberg M. K., Weber I., Warren J. L., Velbel M. A., Tsuchiyama A., Tsou P., Toppani A., Tomioka N., Kazuchige T., Teslich N., Taheri M., Susini J., Stroud R., Stephan T., Staderman F. J., Snead C. J., Simon S. B., Simionovici A., See T. H., Robert F., Rietmeijer F. J., Rao W., Perronnet M. C., Nakamura-Messenger K., Nakamura T., Mostefaoui S., Mikouchi T., Melbom A., Matrajt G., Marcus M. A., Leroux H., Lemelle L., Le L., Lanzirotti A., Langenhorst F., Krot A. N., Keller L. P., Kearsley A.T., Joswiak D., Jacob D., Ishii H., Harvey R., Hagiya K., Grossman L., Grossman J. N., Graham G. A., Gounelle M., Gillet P., Genge M. J., Flynn G., Ferroir T., Fallon S., Ebel D. S., Dai Z.R., Cordier P., Clark B., Chi M., Butterworth A. L., Brownlee D. E., Bridges J. C., Brennan S., Brearley A., Bradley J. P., Bleuet P., Bland P. A., and Bastien R. 2006. Mineralogy and petrology of comet 81P/Wild 2 nucleus samples. *Science* 314:1735–1739.

APPENDIX

Comparison of the Raman Data Between Laboratory Groups

Generated Spectra

Ten test spectra (Fig. A1) were generated to resemble spectra of relatively primitive (Tagish Lake-type) and more metamorphosed (Allende-type) meteoritic IOM (Busemann et al. 2007). See Fig. A1 for the parameter sets. The spectra consist of two pure Lorentzian peaks with a linear or a second order polynomial background. Random noise has been added to some of the spectra (1, 3, 5, 7, 9, and 10). The fitting results for the various Raman groups are given in the Table A1.

In detail, the four test spectra without noise were generally well fitted by all groups. The peak positions ω_D and ω_G are essentially recovered without deviations from the input peak positions (<0.1 Δcm^{-1} in almost all cases). The Tagish Lake-type spectra are slightly more difficult to fit than the Allende-type spectra, the latter having narrower peaks than the former. While all Γ_G values and the Γ_D values of the Allende-type spectra never deviate by more than 3.3 Δcm^{-1} from the input band widths, Γ_D of the Tagish Lake spectrum 4 is generally underestimated by all groups , by up to 17 Δcm^{-1}. The fitted D and G band parameters of the six test spectra with added noise exhibit some more variation than the noiseless spectra. The G band widths show generally small and often random deviations from the input values in the order <0.7 Δcm^{-1}. All fits systematically overestimate ω_G of spectrum 5 by 1.5–1.6 Δcm^{-1}. This is most likely due to a random effect of the added noise. A test sample with 500 spectra of type 5 and randomly added noise yielded a distribution of fitted $\omega_G = (1590.0 \pm 0.8)$ Δcm^{-1}. Hence, spectrum 5 is within 2σ of the average. More severe systematic variations from the input ω_D in all fits are obtained for spectrum 1 (overestimate by ~4–5 Δcm^{-1}) and spectrum 10 (underestimate by ~11–12 Δcm^{-1}). While spectrum 1 shows a flat background, spectrum 10, which has only small peaks, exhibits a steep linear background (Fig. A1). Random noise could be one reason for this deviation, because the fits of spectrum 9, which has a significant non-linear background, exhibit only deviations within 1.4 Δcm^{-1}. However, a steep background cannot be excluded to cause some of the observed deviations.

The most severe divergence from the input parameters is observed for Γ_D and Γ_G. All fits significantly underestimate Γ_D of the Tagish Lake-type spectra by an enormous 79–114 Δcm^{-1}. It is obvious that the steep second order polynomial background of spectrum 9 cannot be

accounted for with the procedures using a linear background approximation. A background correction using a spline instead of a linear background (LANDS) yields better, but still not perfect, results. However, fitting of spectrum 10 with a steep *linear* background also yields Γ_D values that are underestimated by in this case ~45–61 Δcm^{-1}. Comparing spectra 1, 3, 9, and 10 indicates that the extent of the underestimate (mean ~−7, −43, −105, and −3 Δcm^{-1}, respectively) is correlated with the increase of the background. Γ_G values are generally better fitted than the Γ_D values. The various fits agree well with each other, and yield both lower and higher values. Again, the largest variations are found for spectra 9 and 10 with the steepest backgrounds. However, spectrum 10 deviates on average by +17 Δcm^{-1} and spectrum 9 by −15 Δcm^{-1} from the input parameters.

Meteoritic Insoluble Organic Matter (IOM)

The IOM results are given in Table A2. Metamorphic trends are obvious, i.e., the most primitive sample, Cold Bokkeveld, shows the broadest peaks, while the less primitive Leoville and Allende IOM (Alexander et al. 1998; Busemann et al. 2007) exhibits smaller Γ_D and Γ_G values and their band positions are shifted relative to those of Cold Bokkeveld to smaller (ω_D) and slightly larger wave numbers (ω_G), respectively. Those trends are observed in all laboratories and in qualitative agreement with those observed for organic matter in terrestrial and extraterrestrial samples (Beyssac et al. 2003; Djouadi et al. 2003; Quirico et al. 2003; Raynal 2003; Matrajt et al. 2004; Bonal et al. 2006; Busemann et al. 2007).

Relative to the large differences between the samples, the analyses in all five laboratories yield comparable results for Γ_D and Γ_G and ω_G, implying that artifacts due to the experimental setup, e.g., due to laser-induced heating, can be excluded for meteoritic IOM. Note that this does not necessarily imply that the, possibly more fragile, Stardust cometary organics are not affected by laser-induced heating. The results for the D-band position, however, show some discrepancies between various laboratories, that to a certain extent have to be expected because of the different excitation wavelengths of the instruments used. D band positions in various carbonaceous materials are known to be dispersive, i.e., they vary with the exiting photon energy (e.g., Matthews et al. 1999; Ferrari and Robertson, 2001; Negri et al. 2004). Thus, lower D-band positions have to be expected for instruments that used 532 nm excitation rather than 514 nm excitation. Depending on the degree of ordering, amorphization and H content, the D-band positions for various analyzed amorphous carbonaceous materials are reported to down-shift ~5–8 Δcm^{-1} for 532 nm excitation versus 514 nm excitation (Ferrari and Robertson 2001). The first tests on the actual carbonaceous material of meteoritic IOM with 632 nm and 514.5 nm excitation, respectively (at Open University), confirm that meteoritic IOM exhibits dispersion not only in the D-band, but to a lesser degree also in the G-band (see Table A2).

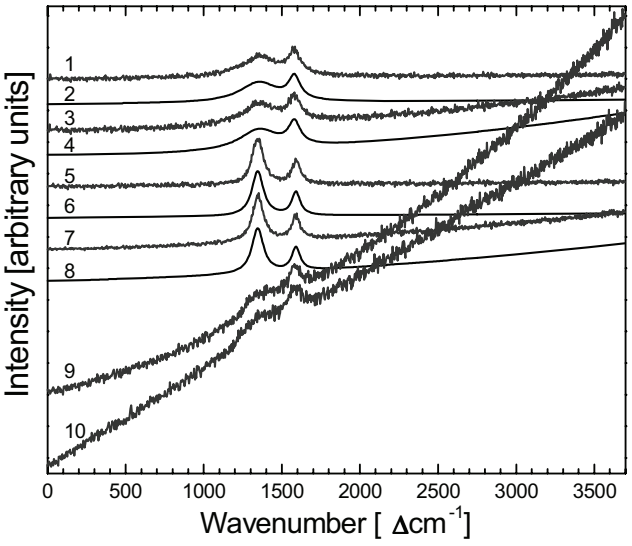

Spectral Parameters (cm^{-1})

	Γ_D	ω_D	Γ_G	ω_G
1	300	1353	90	1580
2	300	1353	90	1580
3	300	1353	90	1580
4	300	1353	90	1580
5	90	1345	65	1590
6	90	1345	65	1590
7	90	1345	65	1590
8	90	1345	65	1590
9	300	1353	90	1580
10	300	1353	90	1580

Fig. A1. Test spectra generated with Raman D and G band parameters typical for primitive (Tagish Lake) and metamorphosed (Allende) meteoritic IOM, consisting of two Lorentzian bands, linear or second order polynomial background, and random noise (noise added to spectra 1, 3, 5, 7, 9, and 10 only).

Table A1. Fitting results (first four rows, D and G band widths Γ and center positions ω) and deviations from input parameters for artificial spectra (given in bold in table header) resembling the spectra of IOM from Allende and Tagish Lake including two Lorentzian peaks for D and G bands and a linear or second order polynomial background. Random noise added to some spectra.

	1 Tagish Lake, linear, noise				2 Tagish Lake, linear				3 Tagish Lake, polynomial, noise				4 Tagish Lake, polynomial				5 Allende, linear, noise			
	300.0	**1353.0**	**90.0**	**1580.0**	**300.0**	**1353.0**	**90.0**	**1580.0**	**300.0**	**1353.0**	**90.0**	**1580.0**	**300.0**	**1353.0**	**90.0**	**1580.0**	**90.0**	**1345.0**	**65.0**	**1590.0**
Team[a]	Γ_D	ω_D	Γ_G	ω_G	Γ_D	ω_D	Γ_G	ω_G	Γ_D	ω_D	Γ_G	ω_G	Γ_D	ω_D	Γ_G	ω_G	Γ_D	ω_D	Γ_G	ω_G
OU	293.2	1357.9	89.4	1580.1	300.0	1353.0	90.0	1580.0	255.1	1355.0	94.2	1579.9	282.7	1352.9	86.7	1579.4	87.1	1345.1	66.5	1591.6
LANDS	283.8	1358.2	87.0	1579.6	296.5	1353.3	91.0	1580.0	254.8	1355.2	94.8	1580.0	292.2	1353.2	89.9	1579.9	87.3	1345.1	66.3	1591.6
IAS	293.7	1357.9	89.3	1580.1	298.1	1353.1	90.6	1580.0	264.1	1354.6	92.2	1580.0	284.7	1353.4	88.7	1579.7	87.4	1345.1	65.3	1591.5
CIW	299.0	1357.6	90.3	1580.3	300.0	1353.0	90.0	1580.0	258.1	1355.4	94.2	1580.2	285.3	1353.0	87.3	1579.5	86.1	1345.3	67.2	1591.6
WU	293.3	1357.9	89.4	1580.1	300.0	1353.0	90.2	1580.0	255.4	1354.9	94.5	1579.9	282.7	1352.9	87.0	1579.4	87.2	1345.1	66.6	1591.6
OU	−6.8	4.9	−0.6	0.1	0.0	0.0	0.0	0.0	−44.9	2.0	4.2	−0.1	−17.3	−0.1	−3.3	−0.6	−2.9	0.1	1.5	1.6
LANDS	−16.2	5.2	−3.0	−0.4	−3.5	0.3	1.0	0.0	−45.2	2.2	4.8	0.0	−7.8	0.2	−0.1	−0.1	−2.7	0.1	1.3	1.6
IAS	−6.3	4.9	−0.7	0.1	−1.9	0.1	0.6	0.0	−35.9	1.5	2.2	0.0	−15.3	0.4	−1.3	−0.3	−2.6	0.0	0.3	1.5
CIW	−1.0	4.6	0.3	0.3	0.0	0.0	0.0	0.0	−41.9	2.4	4.2	0.2	−14.7	0.0	−2.7	−0.5	−3.9	0.3	2.2	1.6
WU	−6.7	4.9	−0.6	0.1	0.0	0.0	0.2	0.0	−44.6	1.9	4.5	−0.1	−17.3	−0.1	−3.0	−0.6	−2.8	0.1	1.6	1.6
	6 Allende, linear				7 Allende, polynomial, noise				8 Allende, polynomial				9 Tagish Lake, polynomial, noise				10 Tagish Lake, linear, noise			
	90.0	**1345.0**	**65.0**	**1590.0**	**90.0**	**1345.0**	**65.0**	**1590.0**	**90.0**	**1345.0**	**65.0**	**1590.0**	**300.0**	**1353.0**	**90.0**	**1580.0**	**300.0**	**1353.0**	**90.0**	**1580.0**
	Γ_D	ω_D	Γ_G	ω_G	Γ_D	ω_D	Γ_G	ω_G	Γ_D	ω_D	Γ_G	ω_G	Γ_D	ω_D	Γ_G	ω_G	Γ_D	ω_D	Γ_G	ω_G
OU	90.0	1345.0	65.0	1590.0	85.4	1346.8	60.6	1589.6	88.2	1345.0	62.2	1590.0	186.8	1351.6	68.8	1579.6	245.2	1341.8	107.9	1580.5
LANDS	90.1	1345.0	64.4	1590.0	86.2	1346.7	58.4	1589.4	89.3	1345.0	64.1	1590.0	220.9	1351.9	84.3	1581.5	254.7	1340.9	106.4	1580.7
IAS	90.0	1345.0	65.0	1590.0	85.6	1346.9	62.3	1589.7	88.4	1345.0	63.4	1590.0	190.7	1353.4	79.0	1580.5	250.3	1341.4	104.3	1580.3
CIW	90.0	1345.0	65.0	1590.0	85.8	1346.8	61.7	1589.7	88.0	1345.0	62.5	1590.0	192.4	1352.4	73.9	1580.1	239.1	1342.0	108.6	1580.3
WU	90.1	1345.0	65.2	1590.0	85.6	1346.8	60.8	1589.6	88.3	1345.0	62.4	1590.0	186.0	1351.7	69.1	1579.6	244.4	1341.7	108.2	1580.5
OU	0.0	0.0	0.0	0.0	−4.6	1.8	−4.4	−0.4	−1.8	0.0	−2.8	0.0	−113.2	−1.4	−21.2	−0.5	−54.8	−11.3	17.9	0.5
LANDS	0.1	0.0	−0.6	0.0	−3.8	1.7	−6.6	−0.6	−0.7	0.0	−0.9	0.0	−79.1	−1.1	−5.7	1.5	−45.3	−12.1	16.4	0.7
IAS	0.0	0.0	0.0	0.0	−4.4	1.9	−2.7	−0.3	−1.6	0.0	−1.6	0.0	−109.3	0.4	−11.0	0.5	−49.7	−11.6	14.3	0.3
CIW	0.0	0.0	0.0	0.0	−4.2	1.8	−3.3	−0.3	−2.0	0.0	−2.5	0.0	−107.6	−0.6	−16.1	0.1	−60.9	−11.0	18.6	0.3
WU	0.1	0.0	0.2	0.0	−4.4	1.8	−4.2	−0.4	−1.7	0.0	−2.6	0.0	−114.0	−1.3	−20.9	−0.4	−55.6	−11.3	18.2	0.5

[a]See title of Table 1 for acronyms of the teams.

All values in cm^{-1}.

Table A2. Raman parameter sets (first six rows) for meteoritic insoluble matter (IOM) from primitive carbonaceous chondrites that experienced distinct thermal metamorphism. The next five rows show the deviations from the mean values, assuming that the standard errors of the means give realistic estimates of the deviation from the true values.

	Cold Bokkeveld				Leoville				Allende			
Team[a]	Γ_D	ω_D	Γ_G	ω_G	Γ_D	ω_D	Γ_G	ω_G	Γ_D	ω_D	Γ_G	ω_G
OU (514 nm)	298.3 ± 19.0	1360.4 ± 2.4	97.5 ± 9.9	1591.6 ± 1.1	169.6 ± 4.7	1350.5 ± 1.0	73.8 ± 2.3	1596.4 ± 1.0	67.1 ± 1.6	1347.5 ± 0.6	61.1 ± 2.1	1596.1 ± 0.6
OU (632 nm)	224.9 ± 11.6	1338.8 ± 6.5	110.7 ± 9.2	1588.2 ± 1.5	185.5 ± 22.4	1324.5 ± 2.0	95.2 ± 10.8	1593.4 ± 2.4				
LANDS (514 nm)	283.4 ± 3.4	1359.4 ± 0.7	92.2 ± 1.0	1592.5 ± 0.3	207.1 ± 3.4	1349.3 ± 0.8	81.1 ± 1.5	1593.9 ± 0.4	71.9 ± 1.1	1348.3 ± 0.3	60.8 ± 1.4	1596.0 ± 0.4
CIW (532 nm)	295.9 ± 29.2	1354.5 ± 6.1	87.2 ± 9.0	1593.0 ± 3.0	210.8 ± 10.3	1342.5 ± 2.2	76.0 ± 3.8	1591.3 ± 2.4	78.6 ± 5.8	1343.1 ± 1.8	66.1 ± 4.2	1591.8 ± 3.8
IAS (514 nm)	267.9 ± 9.9	1364.6 ± 4.3	88.5 ± 1.1	1592.2 ± 2.8	210.7 ± 10.0	1351.2 ± 1.0	80.1 ± 4.1	1591.2 ± 3.5	81.4 ± 6.9	1347.9 ± 1.5	65.4 ± 3.7	1592.7 ± 4.0
WU (532 nm)	254.5 ± 0.9	1361.1 ± 0.2	91.2 ± 0.4	1590.9 ± 0.1	185.5 ± 0.7	1347.2 ± 0.2	78.5 ± 0.4	1591.5 ± 0.1	75.6 ± 0.3	1343.3 ± 0.1	62.8 ± 0.4	1594.1 ± 0.1
Deviation from mean[b]												
OU	18.3 ± 20.5	0.4 ± 2.8	6.2 ± 10.0	−0.4 ± 1.2	−27.2 ± 8.9	2.4 ± 1.7	−4.1 ± 2.6	3.5 ± 1.4	−7.8 ± 2.8	1.5 ± 1.2	−2.1 ± 2.3	2.0 ± 1.0
LANDS	3.4 ± 8.3	−0.6 ± 1.7	0.9 ± 1.9	0.4 ± 0.4	10.4 ± 8.3	1.1 ± 1.6	3.2 ± 1.9	1.0 ± 1.0	−3.0 ± 2.5	2.2 ± 1.1	−2.4 ± 1.7	1.8 ± 0.9
IAS	−12.1 ± 12.5	4.6 ± 4.6	−2.8 ± 2.0	0.2 ± 2.8	13.9 ± 12.5	3.1 ± 1.7	2.2 ± 4.3	−1.7 ± 3.6	6.5 ± 7.3	1.9 ± 1.8	2.2 ± 3.8	−1.4 ± 4.1
CIW	15.9 ± 30.2	−5.5 ± 6.3	−4.1 ± 9.1	1.0 ± 3.0	14.1 ± 12.8	−5.6 ± 2.6	−1.9 ± 4.0	−1.5 ± 2.6	3.6 ± 6.2	−2.9 ± 2.1	2.9 ± 4.3	−2.3 ± 3.8
WU	−25.5 ± 7.7	1.1 ± 1.5	−0.1 ± 1.7	−1.1 ± 0.4	−11.3 ± 7.6	−0.9 ± 1.4	0.6 ± 1.3	−1.4 ± 0.9	0.7 ± 2.3	−2.7 ± 1.1	−0.4 ± 1.1	0.0 ± 0.8
Standard deviation												
	19	4	4	1	18	3	3	2	6	3	2	2

[a]See title of Table 1 for acronyms of the teams.
[b]OU 632 nm measurements excluded.

All values in cm^{-1}.

LANDS = uncertainty from fitting of average spectra of 10, 7, 4 measurements for Cold Bokkeveld, Leoville, Allende, respectively.

IAS = uncertainty from fitting of average of 4, 6, 4 measurements for Cold Bokkeveld, Leoville, Allende, respectively.

CIW = uncertainty standard deviation of mean of 1132, 2731, 1831 measurements for Cold Bokkeveld, Leoville and Allende, respectively.

WU = uncertainty from fitting of 5 spectra for each meteorite.